STUDY OF THE NANOPOROSITY IN CARBON NANOTUBE DISPERSED POLYMER USING POSITRON ANNIHILATION TECHNIQUE

A thesis submitted to
University of Kota, Kota
for the award of the degree of
Doctor of Philosophy
(Physics)
by

SHILPA VIJAY

Under the supervision of

Dr. JAYANT KUMAR VIJAYAVARGIYA
Lecturer
Department of Physics
Government College, Kota

2015

Title of the Thesis	:	STUDY OF THE NANOPOROSITY IN CARBON NANOTUBE DISPERSED POLYMER USING POSITRON ANNIHILATION TECHNIQUE
Name of the Candidate	:	**Shilpa Vijay**
Submitted to	:	Government College, Kota Rajasthan (India)
Faculty	:	Science
Registration Letter No.	:	6 ( ) RS/U.O.K./8999-19000
Registration Date	:	10/11/2011
Thesis Supervisor		**Dr. J. K. Vijayavargiya** Department of Physics, Government College, Kota Rajasthan (India) Phone: +91-9414939830
Place of Work		1. Department of Physics, Government College, Kota-324005 2. Thin film & Membrane Science Lab, Department of Physics University of Rajasthan, Jaipur Rajasthan (India)

DECLARATION

I, hereby, declare that the investigation presented in the thesis has been carried out by me. The work is original and has not been submitted earlier as a whole or in part for a degree / diploma at this or any other Institution / University.

Shilpa Vijay
Department of Physics,
Govt. College, Kota
Rajasthan (India).

Certificate by the Supervisor

Date:

This is to certify that the work entitled **''Study of the nanoporosity in carbon nanotube dispersed polymer using Positron Annihilation''** by Ms. Shilpa Vijay under my supervision for the degree of Doctor of Philosophy (Science) Department of Physics, Government College, Kota.

To the best of my knowledge and behalf, the thesis embodies the work of candidate done by herself, and not yet been reported anywhere. The work fulfils the requirements of the Ph.D. degree.

(Signature of the Supervisor)

Dr. J.K. Vijayavargiya
Department of Physics
Govt. College, Kota
Rajasthan (India)

Contents

Acknowledgements

My accomplishments here during the last four years would not have been possible without the help of several people. They generously guided, assisted, and supported me and I am forever grateful to all of them.

First and foremost I want to express my hearty gratitude to my esteemed guide **Dr. J. K. Vijayavargiya** for his valuable guidance, constant support, encouragement, and motivation throughout the course of this work. I highly appreciate her patience whilst allowing me the liberty to work on my own passion. Above all and the most needed, he provided me unflinching encouragement and patronage in her unique simplicity and cheerful way. Her guidance helped me in all the time of research and writing of this thesis. I could not have imagined having a better advisor and mentor for my Ph.D study.

I am highly thankful **Prof. Y. K. Vijay** for his kind support, encouragement in my research work. This thesis would not have been completed without their continuous support. Again I am thankful Prof. Y. K. Vijay for providing all the facilities in 'Thin film & membrane science laboratory' department of physics, University of Rajasthan, Jaipur during the course of research work.

I am thankful to all scholars Dr. Anshu Sharma, Dr. Balram Tripathi, Dr. Subodh Shrivasatav, 'Thin film and membrane science lab' Department of physics, University of Rajasthan, Jaipur for their cooperation and moral support during the work.

Outside of the teaching world, I would like to thanks my family, my parents Mr. S. N. vijay and Ms. Susheela vijay for their grace and blessings on me to provide me sufficient energy and strength to undertake and complete the present research work. I also gratefully acknowledge the advice and help given by my elder brother's. They provided me all kind of facilities and support during my Ph.D. work.

I would also like to express my deep sense of gratitude to the affection and support shown to me by my cousin. I take this opportunity to dedicate this work to my who gave me consistent support throughout my research.

I would like to thank to all those person whom I came across during my research work for many things that I learnt from them.

Finally I am thankful to all my friends Vinita jain and Archana Jain for their kind support during my Ph.D. work.

I forgot to name plenty of kind people, but I must cut the list somewhere. Excuse me and thank you all.

Above all I owe it all to the almighty god for granting me the wisdom, health and strength to undertake this research work and enabling me to its completion.

Shilpa Vijay

List of Publication

1. **"Frequency and Composition Dependent Dielectric Properties and A.C. Conductivity of Poly methyl Methacrylate/Multiwall Carbon Nanotube",**

   Shilpa Vijay, J. K. Vijayvargiya, Anshu Sharma and Y. K. Vijay, *Advance Science Engineering and Medicine Vol. **5** PP. 1-4,(2013). (www. aspbs.com/asem)*

2. **"Effect of concentration on Electrical and Optical properties of MWNT/PMMA Nanocomposites",**

   Shilpa Vijay, Subhash Chandra, Subodh Srivastava, J. K. Vijayvargiya and Y. K. Vijay**,** International Conference on Nanostructuring by Ion Beams & Schools, Oct. 21-25, 2013.

3. **"Electrical, Optical and Doppler Broadening Spectroscopy Studies of Poly Methyl Methacrylates Acid / Multiwalled Carbon Nanotube",**

   Shilpa Vijay, J. K. Vijayvargiya, Anshu Sharma and Y. K. Vijay**,** *Journal of Advance physics Vol. **5**. PP 1-8, (2016). (www.aspbs.com/jap)*

4. **"Orientation study of Multi wall carbon nanotube dispersed Poly methyl methacrylate acid,"**

   Shilpa vijay, J.K. vijayavargiya and Y.K. Vijay**,** Accept in Polymer/ Metal Nanocomposites Nanowork shop 2015, Vivekanand Global University, Jaipur, Rajasthan, November 2-5, (2015).

Chapter 1

Introduction

Chapter 2

Experimental

Chapter 3

Doppler Broadening Spectroscopy study of MWNT/PMMA nanocomposites

Chapter 4

Electrical, Optical and Surface morphology studies of MWNT/PMMA nanocomposites

Chapter 5

Frequency and Composition Dependence Dielectric Properties and A.C. Conductivity of PMMA/MWNT Nanocomposites

Chapter 6

Conclusion and Future Scope

1.1 Introduction

The word polymer comes from the Greek word, which have many parts. Polymer word describes a long chain molecule with a repeating pattern. However, we live in a world that uses polymeric material on a daily basis. Polymer nanocomposites are composites of polymer matrix and nanoparticles. Current interest in nanocomposites has been generated because nanoparticles and fillers exhibit unique combination of properties. From the mid 1950s nanoparticles have been used to control flow of polymer solution (eg-as paint viscosities) or the constitution of gels. By the 1970s polymer nanocomposites were the topic of text book [1]. Although the term 'nanocomposites' was not in common use.

Important properties of solids depend on both their electronic and defect structure therefore, an experimental and theoretical estimation of these structures is a major task of material science. Thus positron annihilation spectroscopy has found increasing interest and growing application for studying polymeric materials. Doppler broadening spectroscopy of positron annihilation technique is an important tool in the field of materials science. Doppler broadening of annihilation radiation provides a sensitive method of defect characterization by measuring the momentum distribution of the electrons. The addition of carbon nanotube in polymer matrix improves the electrical conductivity, thermal conductivity, optical properties, dielectric properties, and mechanical properties such as stiffness and strength [2]. The nanoparticles are dispersed into the polymer matrix during processing. These materials are better described by the term nanofilled polymer composites.

Nanofiller refer to fillers of 100 nm size in at least one dimension. The small size of the nanofiller can lead to unique and excellent electrical, magnetic, optical, catalytic, mechanical, chemical or biological properties, such as ultra-high modulus and conductivity. Therefore, nanocomposite materials provide the possibility for enhanced functionality in contrast with their single-component counterparts. For example, nanocomposites with altered electrical or mechanical properties that keep their optical clarity can be obtained because very small nanoparticles do not scatter light significantly [3].

In addition, the small size of the fillers leads to an exceptionally large interfacing area in the nanocomposites. Since nanoparticles have a higher surface area per unit volume than larger particles, they have a greater interface with their surroundings. The interface controls the degree of interaction between the nanofiller and the polymer matrix, and thus controls the properties of the nanocomposites show a lower percolation limit and a slower decrease in the resistivity with nanofiller concentration compared to conventional composites. The nonlinear photonic devices by fabrication of carbon nanotube-poly-methyl-methacrylate composites have been investigated. Nanocomposite materials are multi-constituent combinations of nana-dimensional phases with distinct differences in structure, chemistry, and properties. These materials typically contain an inorganic component in an organic host or vice versa.

The motivation behind the present work is to study the investigation of Doppler Broadening Spectroscopy in PMMA (Poly methyl methacrylate acid) Polymer after doping with MWNT (multiwall carbon nanotube) using Positron Annihilations techniques. One of the great successes in this area of research is the determination of micro-structural properties of the defect, such as free volume and holes, on an atomic scale in polymers. Within the Positron Annihilation Spectroscopy (PAS) group, spectral data is being analyzed in order to understand characteristics of a material.

The dielectric behaviors of the MWNT/PMMA nanocomposites were studied by dielectric constant, ac conductivity, dielectric loss and Loss tangent systematically over a range of frequencies. These all properties show the dielectric behavior of MWNT/PMMA nanocomposites. For the present work the MWNT/PMMA nanocomposites have been characterized by various techniques such as XRD, FT-IR, I-V characteristics, Optical microscope etc.

1.2 Carbon nanotube

Since the discovery of CNT (carbon nanotube) by lijima's in 1991[4], CNT have simulated intensive studies for their unique properties extremely high electrical and thermal conductivity, very high aspect ratio and mechanical properties. Many different applications of CNTs have been developed, including their use in nanocsale

fillers. Polymer matrices have been widely exploited as a medium for CNTs. Research projects are focused on the development of CNT-based polymer materials that utilize the carbon nanotubes characteristics and properties, such as:

a) The high strength and stiffness of the CNTs are used for developing superior polymer composites for structural applications which are lighter, stronger, and tougher than any polymer-based material [5].

b) Effort is being made to exploit the electrical conductivity of the CNTs to develop new materials e.g.electromagnetic interference (EMI) shielding, conductive polymers, or antistatic coatings [6]

c) The efficient thermal conduction of the CNT improves the high temperature characteristics of the polymer matrix, by dissipating the heat through the CNTs that prevents the degradation of the surrounding polymer.

1.3 Carbon nanotube polymer nano composites

Many carbon nanotube/polymer composite have been produced and investigated. CNTs have electrical properties that combined with a polymer matrix which lead to conductive polymer composites. Some of the applications that take advantage of the electrical properties of CNTs/polymer nanocomposites are fuel cell, photovoltaic devices such as more efficient solar cells, sensors, field-effect transistors and shottky diodes that improve mechanical stability and conductivity of the devices. Thermal properties are also important in nanocomposites. Glass transition temperature (Tg) and crystalline of polymers have been influenced by the addition of CNTs thus affecting their thermal stability. CNTs in polymeric matrices have shown properties enhancement such as significant increase in tensile strength, yield strength. CNT/PMMA nanocomposites improved thermal and mechanical properties better then pristine PMMA [7]. CNTs have a very low density, comparable to that of polymers. CNTs can be embedded into polymers to make light weight composites with exceptional properties for structural applications.

1.4 Dispersion of CNTs

The practical applications of CNT composites have so far been largely limited by their poor processibility. The intrinsic vander Walls attraction among the tubes in combination with their high surface area and high aspect ratio often leads to significant agglomeration of CNTs. The surface of CNTs is also non reactive which makes it difficult in achieving efficient dispersion, as they mix and blend with the host matrix. To effectively use CNTs as intrinsic reinforcements in composite structures and ensure a good stress transfer between CNTs and the polymer matrix, uniform dispersion within the polymer matrix and improved nanotube/matrix are critical. Different methods have been used to efficiently disperse the CNTs in polymer matrices. Ultrasonication is a very effective method used to disperse CNTs in a solvent before it is added to a polymer matrix. MWNTs in toluene using an ultrasonic wand dismembrator at 300 W for 30 min have been dispersed. Poor dispersion and agglomerations of carbon nanotubes (CNTs) in a polymer nanocomposite resulted in a radically weaker composite.

The dispersion of CNTs is not a simple process since CNTs tend to agglomerate to each other due to the Vander Wall force attractions that exist between the tubes. Therefore, research has considered different methods to well disperse CNTs in polymer matrices. Fornes et al. [8] used chemical modification that consisted in the treatment of CNTs in a solution of acid salt. This solution created electrostatic repulsion forces that separated the tubes. One simple and most convenient method used for dispersion is the ultrasonic or high speed shearing process. Sandler et al. [9] was able to disperse CNTs in a resin by mechanical stirring of the mixture for one hour at 2000 rpm. Truong et al. [10] proved that a proper sonication procedure resulted in well dispersed nanotubes and better composite mechanical properties. In addition, surfactants have been used during the dispersion process to ease the dispersion. Bratcher et al. [11] was able to achieve dispersion when adding a surfactant during sonication. Gong et al. [12] was able to improve the thermo mechanical properties using a surfactant during the processing of polymer nanocomposites.

1.5 Applications of CNT/Polymer Nanocomposites

Since the discovery of carbon nanotubes, they have attracted much interest due to their small dimensions, strength and their exceptional physical properties. Thus, they have been accepted as a unique material with a wide range of favorable scientific and industrial applications.

Together with their light weight, their strength makes nanotubes an ideal candidate for reinforcement in polymer composite materials which have applications in many areas such as the construction of aircraft, space-craft and earthquake-resistant houses and nanoelectromechanical systems (NEMS). Besides the ability of CNTs to reinforce a polymer, CNTs have electrical properties that when combined with a polymer matrix can lead to conductive polymer composites. Some of the applications that take advantage of the electrical properties of CNTs/polymer nanocomposites are super capacitors which are considered for applications such as electric vehicles, fuel cells, uninterruptible power supplies, shielding of electromagnetic interferences, photovoltaic devices such as more efficient solar cells, sensors, field-effect transistors and Shottky diodes that improve mechanical stability and conductivity of the devices.

Previous research works have been found that the addition of SWNTs to polyvinyl alcohol exhibits faster crystallization rate and higher crystallization temperature as compared to pure polyvinyl alcohol. Therefore, CNTs are considered for high temperature applications and for enhancement of thermally conductive paints and coatings applications [13].

1.6 Positron Annihilation Spectroscopy

The positron annihilation spectroscopy has found increasing interest and growing application for studying polymeric materials. This technique uses the interaction between the positron and the e^- from the host material. In polymeric materials free volume holes play an important role in determine a variety of properties of polymers. The positron is an atomic probe and after annihilation gamma photons carry information about the localization sites. Nanoparticles or fillers can fill up the

weak micro region of polymers to boost the interaction forces at the polymer filler interaction [14,15]. A dramatic increase in the interfacial area between fillers and polymer can significantly improve the properties of the polymer.

The positron has positive charge $+e$, spin 1/2, and the same mass m_e as the electron. The positron is emitted in the β decay of radioactive nuclei such as ^{22}Na; however, it was first identified by C.D. Anderson in 1932 in cosmic ray photographs. When a positron interacts with materials, it rapidly associates itself with one of the electrons of the material. In less than 10^{-7} s the positron and electron annihilate to produce two gamma rays in the charge-conserving reaction.

$$e^+ + e^- \Rightarrow 2\gamma \tag{1.1}$$

The energy E_γ of each gamma ray can be computed using conservation of total relativistic energy for a positron and electron initially at rest, that is

$$2mc^2 = 2E_\gamma \tag{1.2}$$

so that,

$$E = mc^2 = \left(9.109\times10^{-31} kg\right)\left(2.99\times10^{8}\frac{m}{s}\right) = 8.14\times10^{-14} J \approx 511 keV \tag{1.3}$$

The positron energy, which extend up to 511 keV decrease in the sample within a few picoseconds by non-elastic interaction. The mean positron penetration depth of this so called thermalization process is of the order of 100 μm [16]. The thermalization time usually amounts to a few picoseconds. Figure 1.1 shows the localization of positronium. During thermalization, a positron may capture an electron from the environmental molecule and form Positronium (Ps), a bound state of positron and electron similar to a hydrogen atom. The polymeric materials contain local free volume, which have the size of few A^o. These are the favorable sites where positron and Ps atoms are localized prior to annihilation.

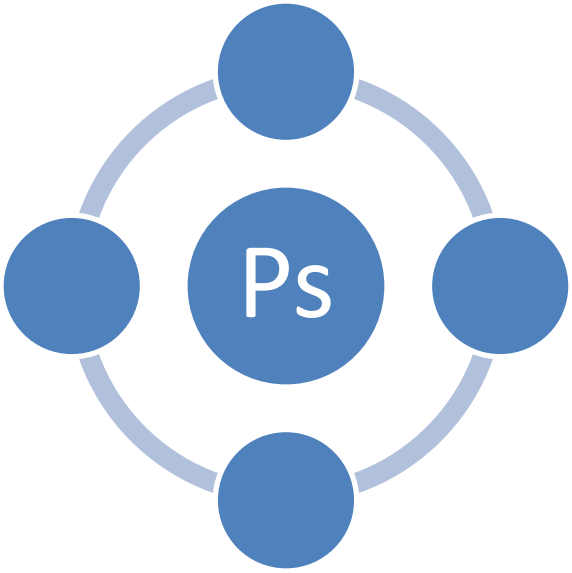

Figure 1.1: Ps localization and annihilation in a hole of the free volume

1.7 PAS Results in Polymer Nanocomposites

The annihilation of positron in condensed matter provides a unique way of obtaining information is transmitted through γ rays, emitted when the positron is annihilated in the material. The internal structure of the material may be probed measuring three fundamental different quantities; (i) angular correlation between emitted γ rays. (ii) The energy distribution of the γ rays and (iii) the lifetime distribution of positron. Metal to semiconductor like transition in polymer nanocomposites can be detected by free volume measurement similar to the electrical resistivity measurements. Gas permeability and selectivity, which depend largely on the porosity of the material is another important area where PAS can certainly provide valuable information. Figure 1.2 shows the all three techniques of Positron Annihilation spectroscopy.

A combined study of variable energy positron life time spectroscopy and Doppler broadening annihilation radiation has been investigated. It is found that the formation of vacancy clusters on the surface of Au nanoparticles embedded in GaAs. The Au implants were not detectable until they form nanoparticles which are associated with vacancy defects. This study clearly demonstrator that the positron probe can be used to characterize defect structure of nanoparticles surfaces [17].

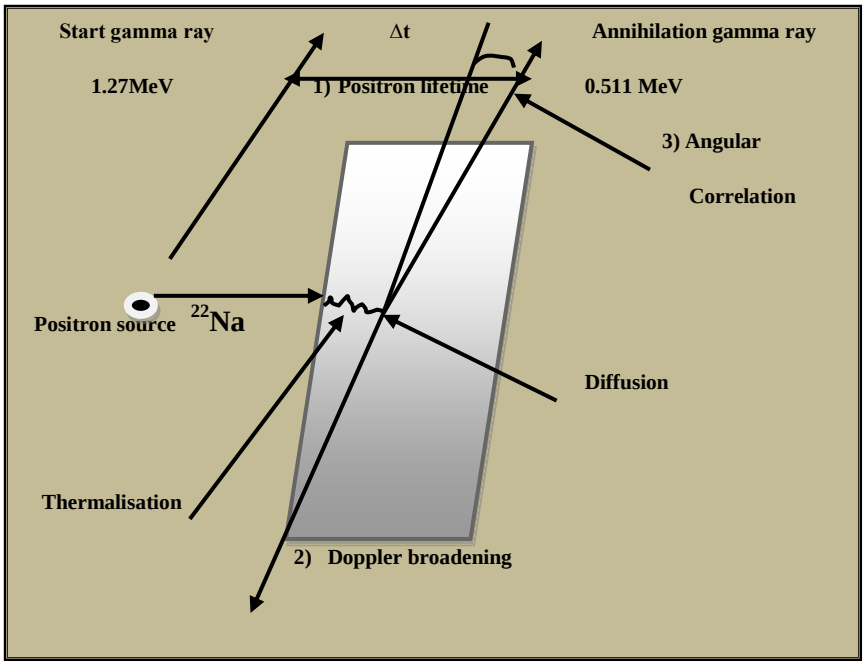

Figure 1.2: Principles of three main techniques in positronannihilation spectroscopy (here presented with ^{22}Na positron source): 1) Positron annihilation lifetime spectroscopy, 2) Doppler broadening spectroscopy and 3) Angular correlations measurements

Furthermore, Positron may get trapped in open-volume defects until they annihilate and exhibit a specific sensitivity to different types of defects.
There are three methods of Positron Annihilation Spectroscopy.

1) Positron Annihilation Lifetime (PAL)
2) Angular Co-relation Annihilation Radiations (ACAR)
3) Doppler Broadening Spectroscopy (DBS)

$$^{22}Na \rightarrow {}^{22}Ne* + e^{+} + \nu \rightarrow {}^{22}Ne + \gamma + e^{+} + \nu_{e}$$

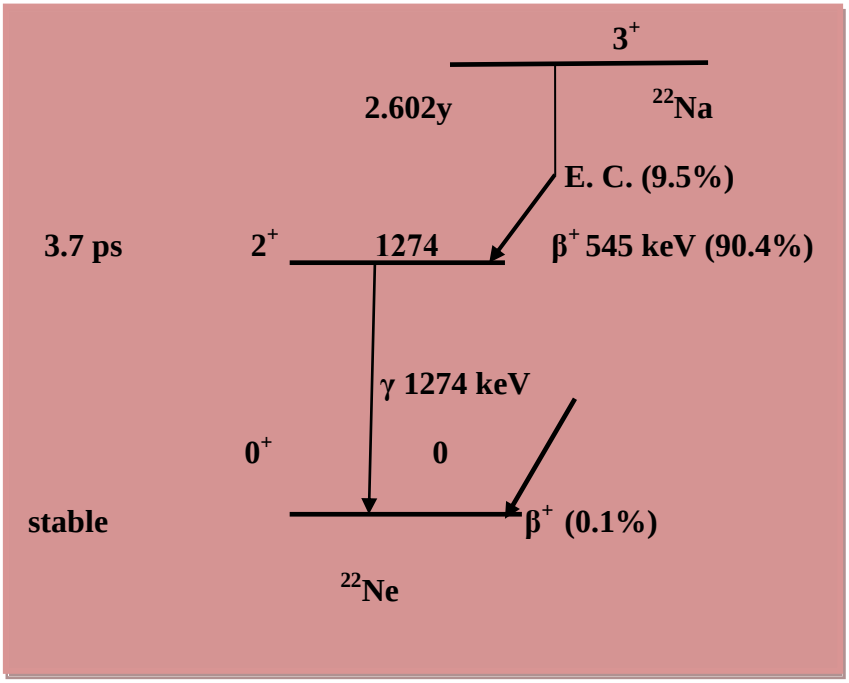

Figure 1.3 : The decay process of ^{22}Na source

Positrons from the sources have a range of energies and can penetrate up to some maximum depth into the sample. On the other hand, positrons from the positron beam can have definite energy and penetration depth, can be used for depth-profiling of the sample. The decay process of ^{22}Na is shown in figure 1.3. After stopping in the material positrons can be either directly annihilated with the surrounding electrons, or if available space permits, can form positronium which eventually annihilates. The annihilation of positronium in material is mainly through so called pick-off process: annihilation of the positron in the positronium with one surrounding electron in the material.

Conservation of momentum during the annihilation process is the reason for the fact that the annihilation radiation contains information on the electron momentum distribution at the annihilation site. This can be used for the study of the electron structure in solids and for the investigation of defects. There are two basic techniques studying the momentum distribution, Doppler-broadening spectroscopy and angular correlation of annihilation radiation. As a result of momentum conservation during the annihilation process, the momentum of the electron–positron pair (p) is transferred to

the photon pair [18]. The momentum component p_z in the propagation direction z of the γ-rays results in a Doppler shift ΔE of the annihilation energy of 511 keV, which amounts approximately to

$$\Delta E = p_Z \frac{c}{2} \tag{1.4}$$

Since numerous annihilation events are measured to give the complete Doppler spectrum, the energy line of the annihilation is broadened due to the individual Doppler shifts in both directions, $\pm z$. This effect is utilized in Doppler-broadening spectroscopy, which is described in Sect. 1.7.3. The momentum conservation during the annihilation process gives a tool to study the momentum distribution of electrons in the solid. The momentum of the positron after thermalization is significantly smaller than that of most electrons. The reason is the Pauli principle and the resulting distribution of the electron momentum up to the Fermi momentum [19-20]. Although the positron is also a Fermi particle, it can thermalize, because there is no more than one positron in the sample at a given time. This allows the probing of the electron distribution in the electron structure in the momentum space. The effect of the localization of positrons in lattice defects enables such a study, not only in the bulk, but also for open-volume defects due to the limited energy resolution of Doppler broadening [21].

1.7.1 Positron Annihilation Lifetime (PAL)

The Positron lifetime measurements is possible since a γ-quanta with energy of 1.27 MeV is emitted almost simultaneously with the positron in the ^{22}Na source. In this case PALS is based on the measurements of the time difference between 1.274 MeV γ- ray, emitted from the daughter ^{22}Ne nucleus almost immediately after positron emission from the ^{22}Na, and one of the annihilated 0.511 MeV γ-rays emitted in positron annihilation. The collected time spectra contain various lifetime contributions and decomposition in individual time components and corresponding intensities can yield information about holes in the sample and their concentrations [22]. This technique, when used with slow positron beam, should include some gating

from the incoming positrons in beam, but with the definite positron energy, the exact penetration depth can be determined.

Annihilation is a random process, thus the positron lifetime, i.e. the time interval between the injection of positron into a sample and the instant of annihilation, has a statistical distribution. In defect-free homogeneous metals, the lifetime spectrum is a simple decaying exponential. In the presence of trapping at defects, the lifetime spectrum becomes a superimposition of decaying exponentials [23-24].

Experimentally, the lifetime of a positron is time delay between the positron emission and annihilation. The 511 keV annihilation photon serves as the stop signal. The lifetime spectrometer consists of a start and stop detector, each of them made by coupling a fast scintillator to a photomultiplier. The timing pulses are obtained by differential constant-fraction discrimination. The time delays between the start and stop signals are converted into amplitude pulses the heights of which are stored into a multichannel analyzer. A typical good time resolution is about 200 ps (FWHM) However, some new systems achieved FWHM on the level 140 ps.

1.7.2 Angular Co-relation Annihilation Radiation (ACAR)

The momentum components p_{xy} perpendicular to the propagation direction lead to angular deviations θ_{xy} of the co linearity of the annihilation γ-rays according to

$$\theta_{xy} = \frac{p_{XY}}{m_O c} \tag{1.5}$$

$m_o c$ is the rest mass of the electron. These equations hold for small angles. θ_{xy} can be registered simultaneously in both x and y directions by a coincidence measurement using position-sensitive detection of the γ-quanta. This technique is known as the angular correlation of annihilation radiation. Since the annihilation γ-quanta are emitted simultaneously, θ_{xy} can be measured in a coincidence arrangement by position-sensitive detectors. As described above, the electron–positron momentum distribution in z direction gives the Doppler shift of the annihilation γ-quanta. As the momentum

distribution is recorded in two dimensions, this technique is referred to as 2D-ACAR [25]. The first ACAR measurements in one dimension were realized with Geiger counters by Behringer and Montgomery (1942). A position-sensitive detection can be realized in the simplest way in one dimension (1D-ACAR) by the mechanical movement of a long scintillation detector (Hautojärvi and Vehanen 1979; Mijnarends 1979).

1.7.3 Doppler Broadening Spectroscopy (DBS)

Doppler broadening spectroscopy (DBS) is the principal technique used to analyze the samples described in this report. The technique examines the Doppler shift in the energy of the gamma radiation resulting from positron annihilation, which is linked to the momentum of the annihilating electrons, and thus properties of the material in which annihilation occur [26-27]. The distribution of electron momentum is expressed in the observed γ spectrum as a Gaussian-like broadening of the 511keV photo peak (Figure 1.4). Typically millions of photons would be measured, and peaks would be 10's of keV in width, however exact measurements are dependent on the material, and the key measurement of positron annihilation spectroscopy.

The broadening of the distribution is dependent on the type of electron with which the positron annihilates. If annihilating in bulk material, it is possible that the annihilation will occur with an energetic core electron from a bulk atom. The higher momentum will cause a wider broadening of the spectrum, in comparison to a positron trapped at a vacancy defect where annihilation with a lower-momentum valence or conduction electron is more likely.

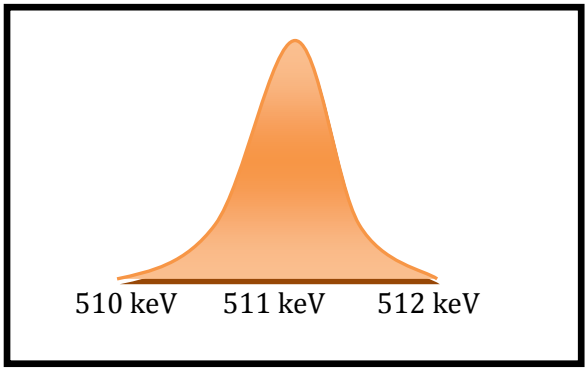

Figure 1.4: Doppler broadening peak at 511 KeV

Generally, the larger the defect, the lower the mean momentum of the annihilating electron, the less pronounced the broadening, and the sharper the peak.

In DBS (Doppler Broadening Spectroscopy) the interest is focused on the 511 keV line, which is Doppler-broadened due to the momentum component p_z of the e+ and e^- pair, where *z* is the detection direction. The peak is a superposition of a narrow (approximately a Gaussian) component due to the self-annihilation of Para-positronium (p-Ps) and broader Gaussian-like distributions due to free e+ and o-Ps pick-off annihilation. The narrow component reflects the localization momentum of the p-Ps inside FVH (Free Volume Hole) and according to the Heisenberg uncertainty principle; it is sensitive to the FVH size [28].

The motion of the annihilating pair causes a Doppler shift. This causes the broadening of the 511keV annihilation line. The shape of the 511 keV peak is in fact the one-dimensional momentum distribution of the annihilation radiation. The Doppler broadening is experimentally measured using a Ge gamma detector. For measurements of bulk specimens, the same source-sample sandwich is used as in the lifetime experiments. The typical resolution of a detector is around 1 keV at 500 keV. This is considerable compared to the total width of (2-3) keV of the annihilation peak meaning that the experimental line shape is strongly influenced by the detector resolution. The most practical scheme still is to use various shape parameters to characterize the 511 keV line.

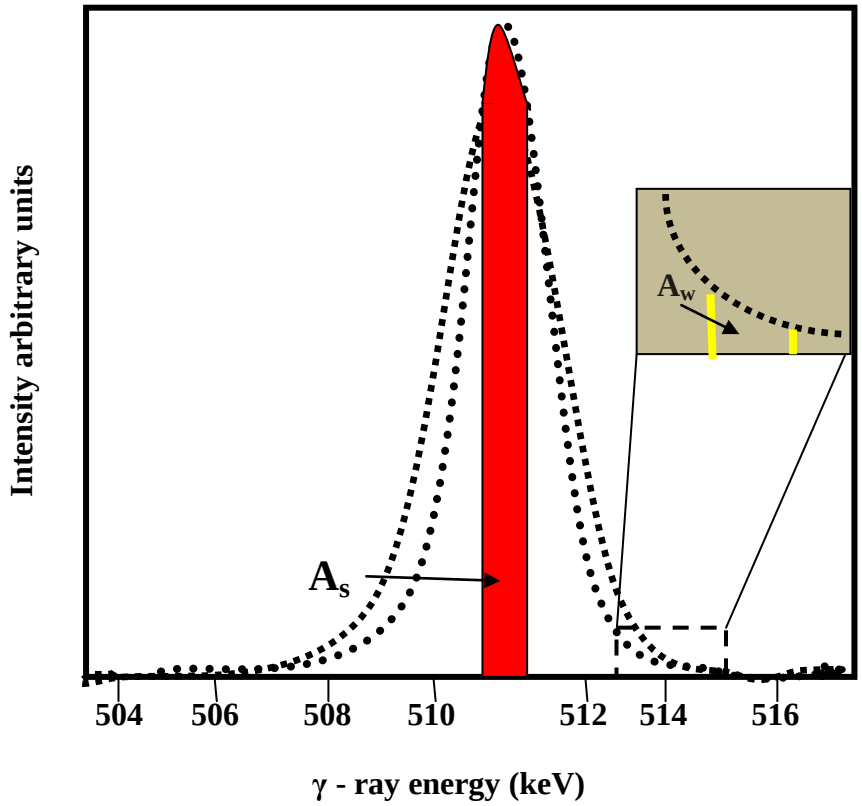

Figure 1.5: Doppler broadening spectra of as- grown zinc doped gallium arsenide compared with plastically deformed GaAs (Hubner et al. 1997). The line shape parameter S and W are determined by the indicated area A_s and A_w divided by the area below whole curve.

The quantitative evaluation can be carried out with specific line shape parameters. The S- parameter is defined as the area of the central low-momentum part of the spectrum, A_s, divided by the area below the whole curve A_o after background subtraction, The central window for S- parameter is chosen so that it cover about 50% of the total peak (S~0.5).

$$S = \frac{A_s}{A_o} \tag{1.6}$$

The W- parameter is taken in a high-momentum region far from the center, as indicated in Figure 1.5. It is calculated as the area of the curve in a fixed energy interval, A_w, divided by A_o,

$$W = \frac{A_w}{A_o} \tag{1.7}$$

Due to their low momentum, the annihilations with valence electron fall predominantly in the region of S- parameter. Mainly core electrons have momentum values high enough to contribute to the W- parameter, respectively. In order to get maximum information out of the parameters, a proper choice of the energy windows is important. The W- parameter window should be far enough from the peak to ensure that mainly core annihilations are accepted.

M. E. Seaman et al. [29] show that the free volume measured by DBS changes with the type of filler added. It is found that that the S- parameter depends on the morphology of the filler and to the filler-rubber interface interaction.

Hamdy et al. [30] have been studied that the Doppler Broadening of Annihilation Radiation of pure Al_2O_3, pure PVC and doped PVC with different concentration of Al_2O_3. The CDBAR curves with respect to pure PVC were presented and reflect the momentum distribution of the entire sample.

Jeevananda et al. [31] show that the free volume can provide interesting information that co relate with the electrical and thermal properties of the HDPE/MWNT nanocomposites. As the MWNT content increase, the resistivity of the nanocomposites significantly decreased. The free volume data further suggested that the micro structural properties co-relate with the macro-characteristics of the nanocomposites.

1.8 Dielectric Material

The electric circuit cannot be composed without conducting and electrical insulating materials. Dielectric materials offer a very high resistance to the passage of electric current under the action of applied direct-current voltage and therefore, different in their basis electrical properties from conductive material under the action of alternatively voltage any dielectric material will pass alternatively capacitance current. It is required to know not only their electrical properties but also their general physical and chemical properties [32]. The dielectric studies have made important

contribution to the fundamental research. Dielectric materials play an important role in defense data sensing navigation and communication through electric means. The dielectric parameters of such materials are therefore extremely important.

Most polymers used in microelectronic industry such as PMMA, PC, Silicones, Benzocyclobutenes (BCB), and Polyimide's (PI) are available for various applications. Generally, polymers have low dielectric constant in the range of 2-5, e.g., ~ 2.5 for polystyrene, ~ 2.65 for BCB, ~2.7 for parylene, ~2.72 for silicone, and ~ 3.5 for epoxy and polyimide. As one of the most primarily used polymers in electronic industry is PMMA, which have been of particular interest for embedded capacitor applications. The dielectric constant of PMMA can be adjusted by disperse the nanoparticles in PMMA matrix. For example, the dielectric constant of epoxy system can be increased significantly from 3.2 to 20.0 by addition of the nanofiller. Compared with conventional polymers, ferroelectric polymers can have higher dielectric constant (ε) values, above 10, because of its polar backbone. For example, pure polyvinylidene fluoride (PVDF) polymer has a ε of about 11 at 1 kHz and Poly (vinylidene fluoride-trifluoroethylene) (PVDF-TrFE)) copolymer, a class of relaxer ferroelectric, can have a relatively high ε around 40 at room temperature after irradiation treatment [33]. In the case of a conductive polymer with conjugated backbone, the ε can be even higher. For instance, polyaniline (PANI) was reported to possess a ε value larger than 104 in a partially crystalline system for which an inhomogeneous disorder model was proposed [34-35].

The study of dielectric properties of polymer nanocomposites materials are of considerable interest. As electrical components are miniaturized, the need for well characterized dielectric measurement on thin material is in great demand. Dielectric studies of polymer composites at different frequencies provide information on the molecular configuration of a system. The dielectric properties of polymer nanocomposites are studied by its interaction with electromagnetic field. When polymer substance is subjected to electric field, polarization phenomena occur. The electric field causes a small displacement of electrons, which produce an induced electric moment in the molecule. The electric moment persists during the whole time

for which the field is applied. The displacement of polar groups requires some time and is thus dependent on frequency, At frequencies, where dispersion occurs, only a part of the entering electric energy is stored which is proportional to the dielectric permittivity which some energy is lost which is proportional to the dielectric loss.

D.C Tiwari et al. [36] have been observed the dielectric permittivity and dielectric loss of nanocomposites by dispersing conducting particles in polymer matrix. They conclude that incorporating MWNTs in to a polymer matrix to form nanocomposites increase the conductivity by 10 times. It is observed that incorporating MWNTs into PTH modifies the electrical behavior and almost metallic type of behavior of this nanotube gives rise to a conducting polymer nanocomposites material. MWNT can be used for solar cell application.

T. Estabrak et al. [37] have been investigated the a.c. electrical and dielectric properties of Polyvinyl Chloride (PVC) with Multi-Walled carbon nanotube (MWCNT) nanocomposites for different concentration and temperature in the frequency range.

2.1 Introduction

This chapter provides a description of materials, fabrication of MWNT/ PMMA nanocomposites and their characterization techniques used for the present work.

2.2 Materials used

2.2.1 Carbon Nanotubes (Multi-walled carbon nanotube)

MWNT (~ 10-30 nm diameter, 1-2 μm length) were acquired from Helix material solution Richardson, Texas. Multi-walled nanotube can appear either in the form of a coaxial assembly of SWNT similar to a coaxial cable, or as a single sheet of graphite rolled into the shape of a scroll. The diameter of MWNT is in the range of 5 nm to 50 nm. The interlayer distance in MWNT is close to the distance between grapheme layers in graphite. MWNT are easier to produce in high volume quantities than SWNT. However the structure of MWNT is less well understood because of its greater complexity and variety.

2.2.2 Poly methyl methacrylate (PMMA)

PMMA (Poly methyl methacrylate): is a transparent, polar, strong amorphous polymer. It has a wide range of application in industrial and domestic applications. Its transparency make it a promising material for several optical applications like windows of aeroplane, lenses for automobile lighting, ventilators, transparent dome, etc. It is also used in optical fibers, biological specimen preservations, dentures, contact lens, etc. It is obtained by polymerization of methyl methacrylate [41]. The structural formula of PMMA is shown in Figure 2.1.

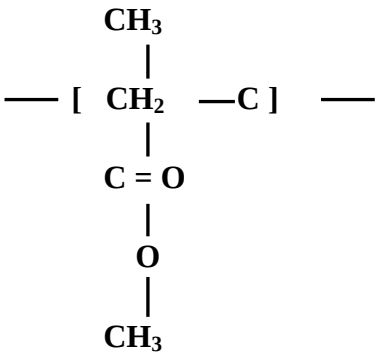

Figure 2.1 Chemical structure of PMMA (Poly methyl methacrylate)

It transmit more light (up to 93% of visible light PMMA exhibits) then glass. Unlike glass, PMMA does not filter ultraviolet light. It transmits UV light down to 300 nm and allows infrared light of up to 2800nm to pass.

2.2.2.1 Properties

➢ Density	1.15-1.19gm/cm^3
➢ Tensile strength	47-79 MPa
➢ Tensile modulus	2.2-3.8 GPa
➢ Electrical resistivity	10^{14} -10^{15} Ω-cm
➢ Dielectric Constant	2.8-4
➢ Thermal conductivity	0.19-0.24 W/m.K
➢ Glass transition temperature	100-105 ^oC
➢ Tranmission, visible	80-93%
➢ Refractive index	1.49-1.498

The range given in the table indicates the minimum and the maximum value of the respective property.

2.2.2.2 Application

PMMA is an economical, versatile general-purpose material. It is available in cast material in sheet, rod and tubes forms as well as custom profile. Various types of acrylics are used in a wide variety of fields and application, including [42]:

- Optics: Sunglasses, watch glasses, lenses, magnification glasses;
- Vehicles: Indicators, Tachometer covers, warning triangles;
- Electrical: Lamp cover, switch parts, dials, control buttons;
- Medicine: Packaging for tablets, pills, capsules, urine containers;
- Others: Leaflet dispensers, shower cubicles, transparent pipelines, toys.

2.3 Preparation of CNT/Polymer composite membrane

For the present work we have prepared polymeric membrane of PMMA matrix membranes with CNTs using solution casting method. The polymeric

membranes can be made by different techniques. It may be classified mainly into two categories: Melting method and Solution casting method. In the present work composite membranes were prepared by solution casting method [43]. It is usually important in dissolving polymers to have the material as finely divided as possible and to have each particle thoroughly wetted by the solvent. Agitation of some kind is important, since the solvent penetration is very slow for high molecular weight polymers and a viscous coating is usually formed over each particle, which retards further solvent diffusion into the polymer.

In this process, polymers (PMMA) were dissolved in the suitable solvent according to the solubility of the polymer using magnetic starrier for 3 hours. The CNTs (MWCNT) were dispersed in same solvent to make the their homogenous suspension using Ultrasonication for 2 hours and then this homogenous suspension was mixed with prepared polymeric solution to make the composite solution by further ultrasonication and then magnetic starrier for 1hr. This composite solution was pursed in flat bottom glass petrie dish floating over mercury to prepare the composite membrane and it was left over night. The schematic diagram of step wise membrane preparation process is shown in Figure 2.2

a) Dissolve the PMMA in the proper solvent using magnetic steerior for a 3 hour.

b) Dispersed the MWNT in the same solvent and make the homogeneous MWNT suspension by ultrasonication for 2 hour.

c) Add the homogeneous MWNT suspension with the as prepared polymer solution by ultrasonication for 1 hour and then magnetic sterior for 1 hour.

d) This composition solution was pursed in flat bottom glass petric dish floating over mercury for preparation composite membrane removable of solvent.

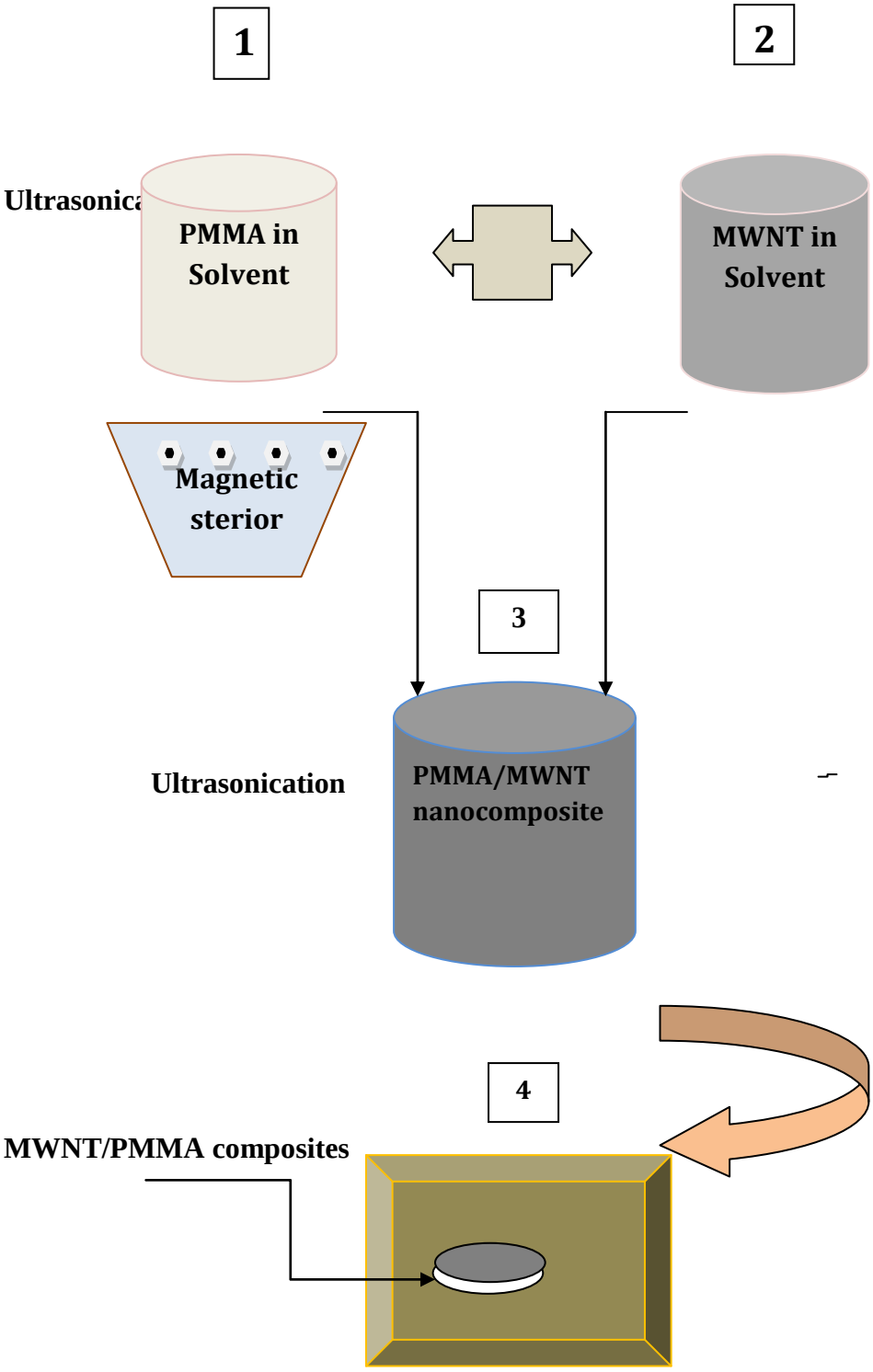

Figure 2.2: Schematic diagram of step by step preparation process of CNT/ Polymer composite membrane using solution mixing method

2.4 Characterization Techniques

Synthesized multiwall carbon nanotubes/polymethyle methacrylate (MWNT/PMMA) nanocomposites were analyzed using different characterization techniques like XRD, FTIR, Raman, Optical Micrograph, SEM, UV-VISIBLE, I-V Characteristics, Dielectric properties and Doppler broadening spectroscopy. These characterization techniques with their working principle and specifications have been discussed in following subsections.

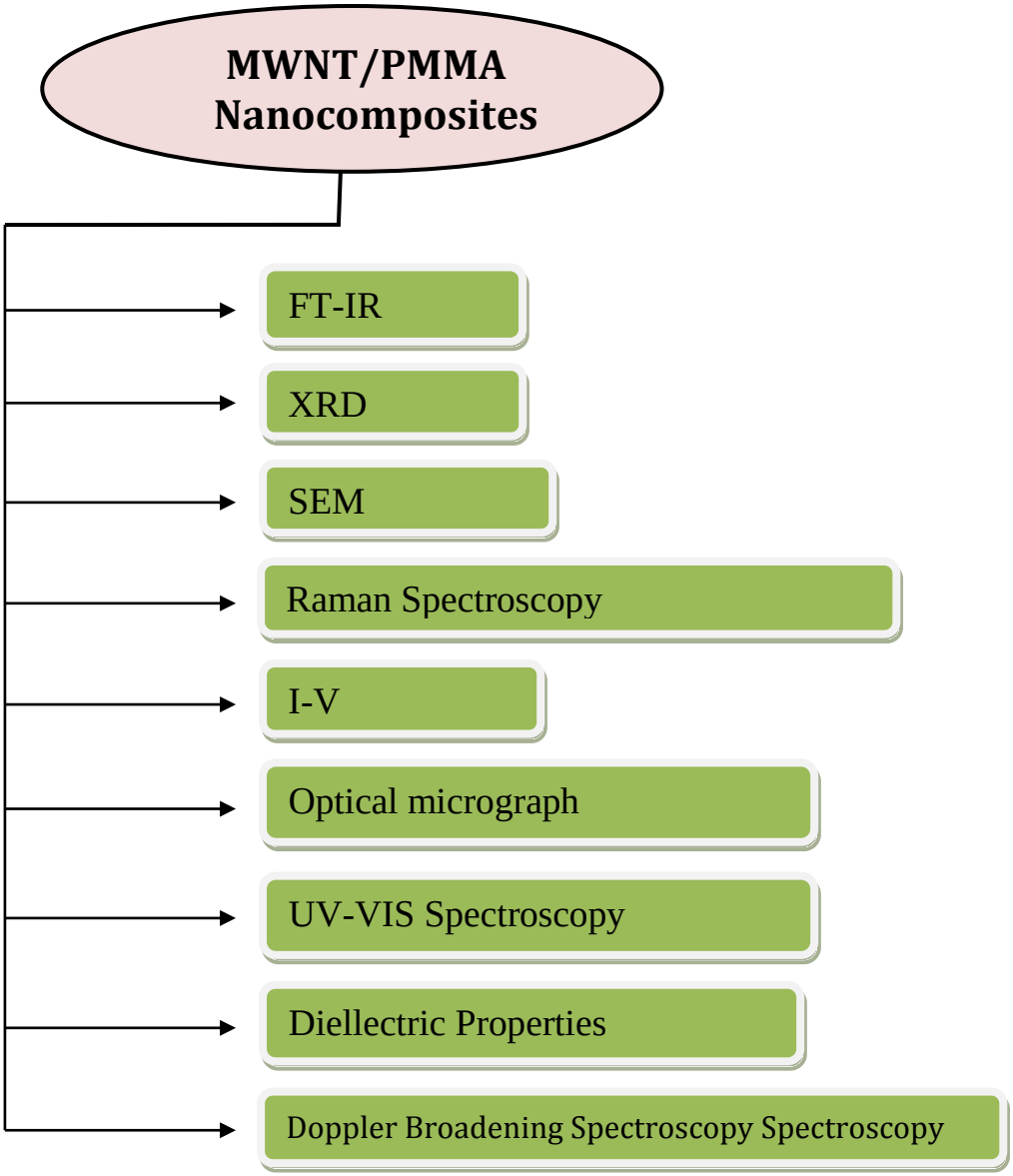

Figure 2.3: Various Characterization technique of MWNT/PMMA Nanocomposites

2.4.1 X-ray Diffraction

X-Ray Diffraction (XRD) is a powerful technique used to identify the crystalline phases present in materials and to measure the structural properties (strain state, grain size, epitaxy, phase composition, preferred orientation, and defect structure) of these phases. XRD is noncontact and nondestructive, which makes it ideal for in situ studies. To identify uniquely the crystalline phases near solid surfaces, X-ray diffraction is used under glancing incidence geometries, which limit the penetration of the beam and enhance the diffraction pattern of the film with respect to the substrate. In general all materials are categorized into crystalline and amorphous materials. Crystalline materials have a patterned arrangement of atoms that can extend in all three dimensions. The extended structure could be described by a basic repeat unit of atoms in the long-range unit cell, which is defined by how the atoms pack in the extended structure. Based on the kind of packing, they can be categorized as simple cubic, body centered cubic (BCC), face centered cubic (FCC) and hexagonal close packed (HCP). These are the more common types of arrangement. Amorphous materials on the other hand lack a systematic and regular arrangement of atoms over relatively large atomic distance.

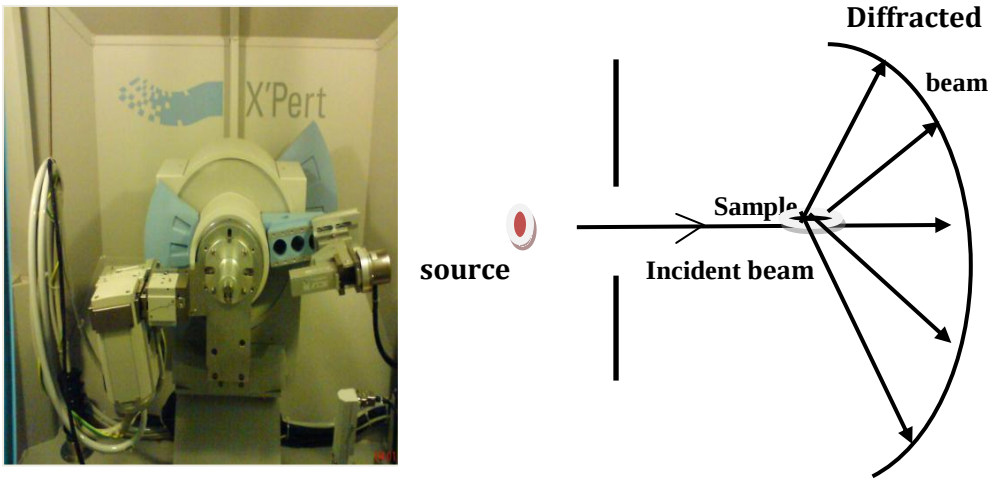

(a) (b)

Figure 2.4: (a) X-ray Diffractometer and (b) diffraction phenomenon.

Crystalline-Size Determination

Scherrer [44] first showed that the mean dimension D, of the crystallites is related to the pure X-ray diffraction broadening β (FWHM of the diffraction peak) by the equation,

$$\beta = \cos 89.0D = \beta$$

bove equation is known as Debye-Scherrer equation.

In present work the structural studies were carried out by X-ray powder diffractometer as shown in Figure 2.5(a) (Model: PANalytical X'pert PRO MPD PW3040/60) with CuK $\lambda = 1.5418A^{o}$ for Bragg angle 10<2θ<60. The tube was operated at 45 kV, 40 mA with a scanning rate of 1degree/min. The peaks of the XRD patterns were searched by computer programming using Powder X Software. These measurements have been done at Department of Physics, University of Rajasthan, Jaipur.

2.4.2 Fourier Transform Infrared Spectroscopy (FT-IR)

Infrared (IR) spectroscopy is a useful technique for characterizing materials and providing information on the molecular structure, dynamics, and environment of a compound. When irradiated with infrared light (photons), a sample can transmit, scatter, or absorb the incident radiation. In infrared spectroscopy, IR radiation is passed through a sample. Some of the infrared radiation is absorbed by the sample and some of it is passed through (transmitted). The resulting spectrum represents the molecular absorption and transmission, creating a molecular fingerprint of the sample. Like a fingerprint no two unique molecular structures produce the same infrared spectrum. This makes infrared spectroscopy useful for several types of analysis. It can identify unknown materials, determine the quality or consistency of a sample and it can determine the amount of components in a mixture.

Many functional groups vibrate at nearly the same frequencies independent of their molecular environment. This makes infrared spectroscopy useful in materials characterization. Further, many subtle structural details can be gleaned from

frequency shifts and intensity changes arising from the coupling of vibrations of different chemical bonds and functional groups [45].

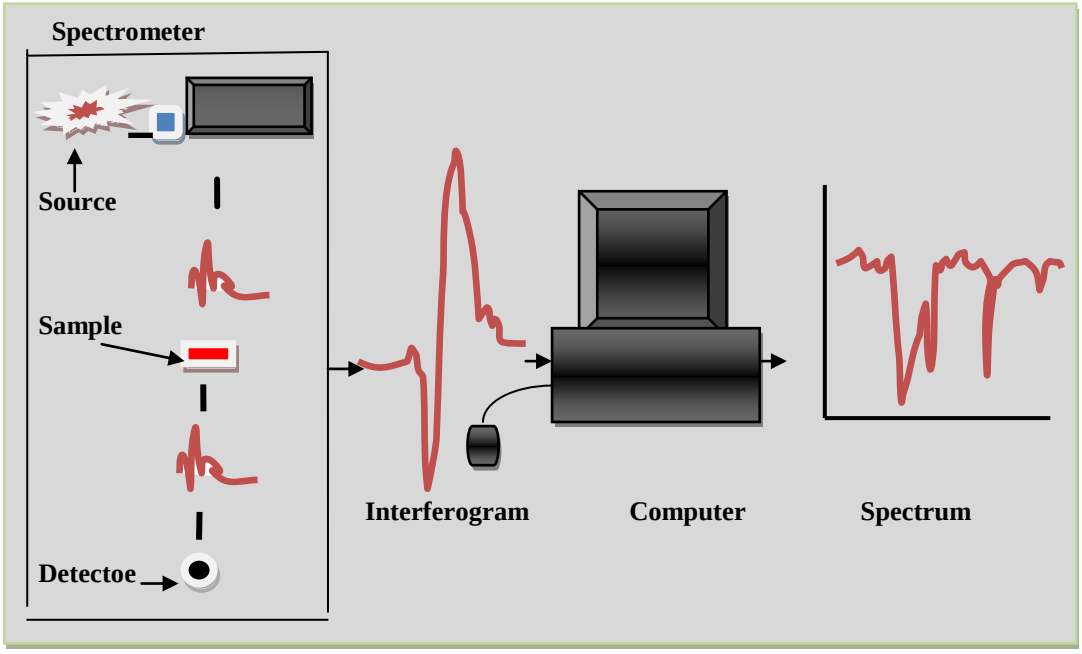

Figure 2.5: Diagram of a FT-IR spectrometer.

Because there needs to be a relative scale for the absorption intensity, a background spectrum must also be measured. This is normally a measurement with no sample in the beam. This can be compared to the measurement with the sample in the beam to determine the percent transmittance. This technique results in a spectrum which has all of the instrumental characteristics removed. Thus, all spectral features which are present are strictly due to the sample. FTIR spectroscopy was performed in absorption mode using FTIR SHIMADZU spectrometer at University Science and Instrumentation Centre, University of Rajasthan, Jaipur. The spectra were recorded in the wave number range of 500-3500 cm-1.s

2.4.3 UV-VIS Spectroscopy

The UV-VIS measurement were carried out on a UV-1601 PC spectrometer in transmission mode in the wavelength range of 300-900 nm having resolution 2.0 nm and spectral bandwidth 2.0nm. Block diagram of UV-VIS is shown in fig 2.6. The UV-1601 combines optical performance with an unprecedented choice of personal

computer (PC) operation. The double beam design offers the best in modern grating technology with the mono chromator mounted on to a high stable optical bench to ensure integrity and trouble-free operation. Further improvement in long-term stability is achieved through automatic monitoring and adjustment for fluctuation in lamp output and system electronics. The blazed holographic grating with self-aligning, energy optimizing deuterium and tungsten-halogen lamps enhances precision across the UV-VIS spectrum. Spectral data is obtained at constant band pass with resolution of less than 2nm.

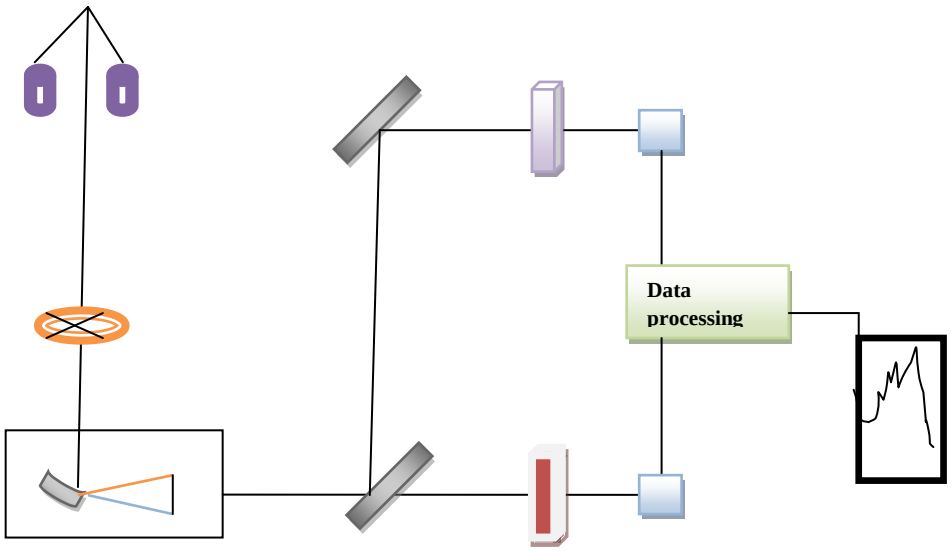

Figure 2.6: Block diagram of UV-VIS spectroscopy

2.4.4 Optical Microscopy

The surface morphology of thin film was studied by optical micrograph. The optical microscope magnifies an image by sending a beam of light through the object as shown in Figure 2.7. The optical assembly nearest the eye, the eyepiece further magnifies the magnified image formed by the objective, so-called primary image. An eyepiece does little to the primary image other than make it visible to eye. The condenser lens focus the light on the sample and the objective lens (4x, 10x, 40x and 100x) magnifies the beam, which contains the image, to the projector lens so the image can be viewed by the observer.

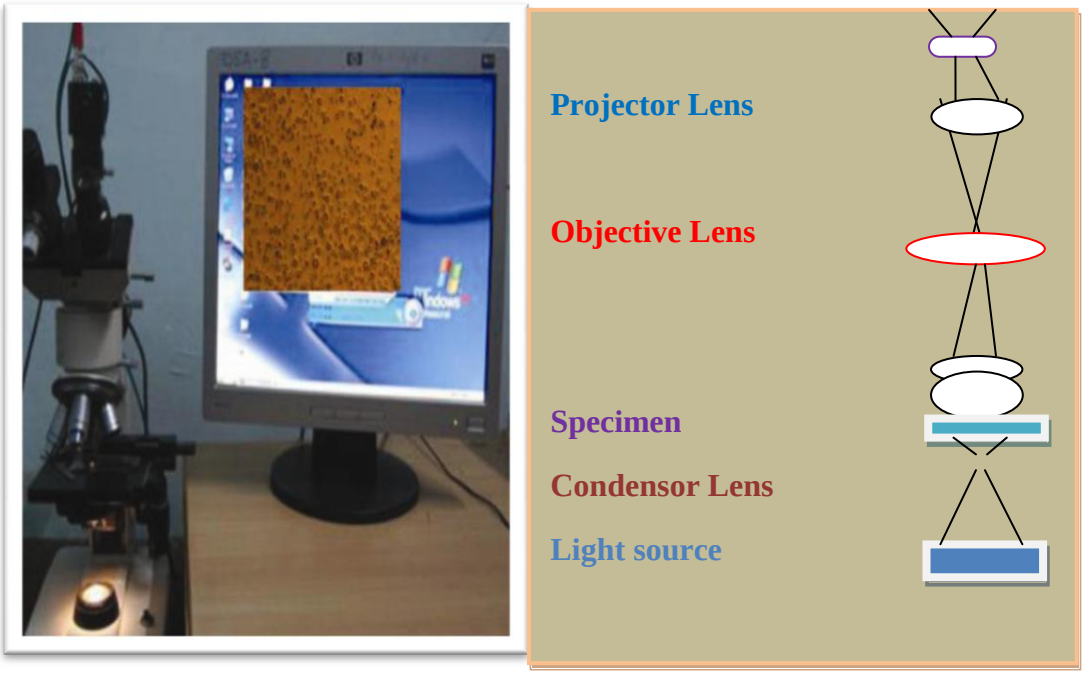

Figure 2.7: set up and block diagram of Optical Micrograph

The optical micrographs have been taken with Microscope. The micrographs are stored in computer through CCD camera, which is attached to computer with standard software. The scale on micrographs can be determined on comparing with electron microscopic grid. It is a circular grid having 3 mm of diameter and there are thousand small squares in 7.06 mm2 area.

For the present study the optical micrographs were taken with the help of Labomed optical microscope at 10x magnification having resolution of the order of 1m and the microscope was kept in reflection mode. The micrographs were stored in computer through standard software Pixel View. Recorded two-dimensional (2-D) optical micrographs were converted in three-dimensional (3-D) images with the help of Scanning Probe Image Processing computer program.

2.4.5 Scanning Electron Microscope (SEM)

The scanning electron microscope (SEM) uses a focused beam of high-energy electrons to genesrate a variety of signals at the surface of solid specimens. The

signals that derive from electron-sample interactions reveal information about the sample including external morphology (texture), chemical composition, and crystalline structure and orientation of materials making up the sample. In most applications, data are collected over a selected area of the surface of the sample, and a 2-dimensional image is generated that displays spatial variations in these properties. Areas ranging from approximately 1 cm to 5 microns in width can be imaged in a scanning mode using conventional SEM techniques (magnification ranging from 20X to approximately 30,000X, spatial resolution of 50 to 100 nm).

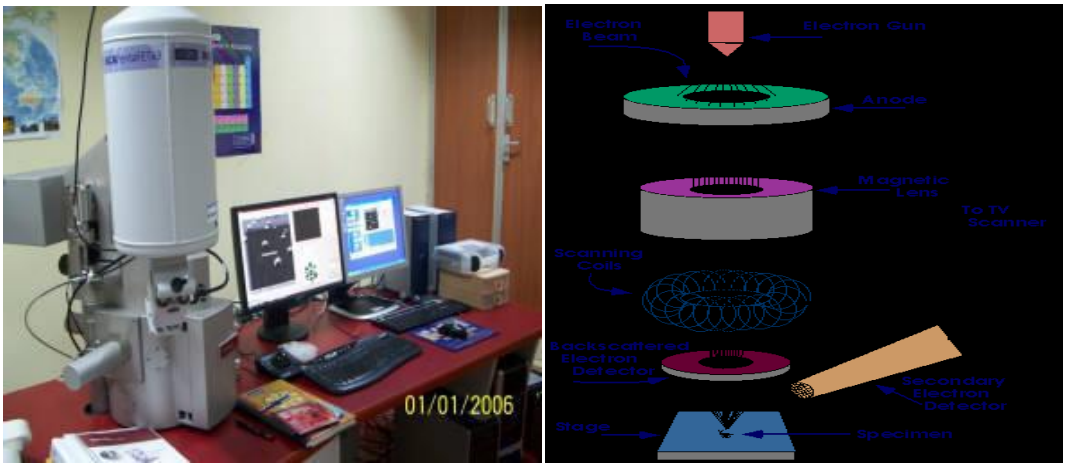

Figure 2.8: (a) & (b) Schematic representation of SEM

Principle of SEM

Accelerated electrons in an SEM carry significant amounts of kinetic energy, and this energy is dissipated as a variety of signals produced by electron-sample interactions when the incident electrons are decelerated in the solid sample. These signals include secondary electrons (that produce SEM images), backscattered electrons (BSE), diffracted backscattered electrons (EBSD that are used to determine crystal structures and orientations of minerals), photons (characteristic X-rays that are used for elemental analysis and continuum X-rays), visible light (cathodoluminescence-CL), and heat.

Secondary electrons and backscattered electrons are commonly used for imaging samples: secondary electrons are most valuable for showing morphology and topography on samples and backscattered electrons are most valuable for illustrating

contrasts in composition in multiphase samples (i.e. for rapid phase discrimination). X-ray generation is produced by inelastic collisions of the incident electrons with electrons in discrete ortitals (shells) of atoms in the sample. As the excited electrons return to lower energy states, they yield X-rays that are of a fixed wavelength (that is related to the difference in energy levels of electrons in different shells for a given element). Thus, characteristic X-rays are produced for each element in a mineral that is "excited" by the electron beam. SEM analysis is considered to be "non-destructive"; that is, x-rays generated by electron interactions do not lead to volume loss of the sample, so it is possible to analyze the same materials repeatedly.

2.4.6 Thermal evaporation unit

Figure 2.9: Vacuum thermal evaporation unit

Thermal evaporation is one of the widely used metal deposition technique. Thin films are made by vaporizing a solid material by heating it to sufficiently high temperature and recondensing it on a cooler substrate. Passing a large current through a resistive element generates sufficient heat to melt and evaporate various coating materials.

Once the metal is evaporated, its vapor undergoes collisions with the surrounding gas molecules inside the evaporation chamber. Due to this reason, good vacuum is also a prerequisite for producing contamination free deposition. Thus the mean free path of the evaporated molecule is longer than the distance between the evaporation source and the

sample holder. For deposition of interdigited aluminum electrodes, a tungsten boat is filled with highly pure aluminum granules. This aluminum-loaded boat is clamped in between the copper rods which are connected to high current source. The cleaned glass substrates are properly masked so as to define an interdigited electrode deposition. After attaining vacuum of about 10^{-6} torr, the aluminum loaded tungsten filament is heated by passing AC current through the heating electrodes. This causes aluminum evaporation and vapor so formed when comes in contact with the masked substrate, gets condensed and forms a thin film of Al with very high purity and stability. The thermal evaporation unit used in the present work is shown in Figure 2.9.

2.4.7 I-V Characterization

The electrical conductivity can be measured by several techniques. In the present study two-probe method has been used. I-V characteristics of samples have been recorded by using Keithley-238 high current source measuring unit. For I-V characteristics, electrode contacts have been made using silver paste on the thin films. All the measurements have been performed at room temperature. Schematic diagram of I-V characteristics set-up is shown in Figure 2.10.

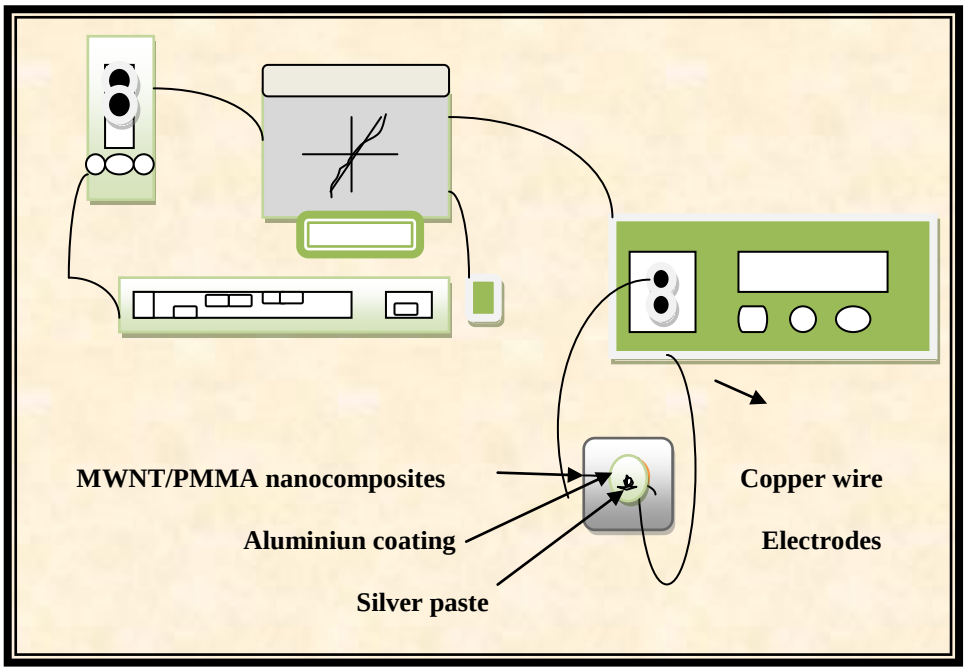

Figure 2.10: Block diagram of I-V measurement set-up

2.4.8 Dielectric constant

Frequency dependent dielectric measurements have been used in order to measure the dielectric constant of the randomly oriented CNT/PC nanocomposite films and oriented CNTs in PC matrix. Aluminum is vapor deposited on these nanocomposite membranes as electrodes on the surface of the films. MT-4080 Handheld high precision LCR meter is used. The dielectric constant is measured across the thickness of the nanocomposites and it is measured in frequency range of 100 Hz to 10 kHz at room temperature. The dielectric constant (ε) is used to define the ability of an insulator to store electrical charge. For parallel capacitive electrodes, the permittivity of media material can be obtained from capacitance:

$$C = \frac{A\varepsilon_0}{d} \tag{2.1}$$

where C and d are capacitance and distance between the electrodes, respectively; ε is dielectric permittivity of media material and A is the area of the electrodes. The relative permittivity ε_r of the media material is the ratio of permittivity over that of free space ε_o:

Figure 2.11: Dielectric measurement set-up

2.4.9 Dielectric measurement (conductivity, Loss factor, etc)

The Agilent E4980A LCR meter, as shown in Figure 2.12, is used with a 16451 dielectric test fixture assembly. The Agilent E4980A is a general-purpose LCR meter for incoming inspection of components, quality control, and laboratory use. The E4980A is used for evaluating LCR components, materials, and semiconductor devices over frequency from 20 Hz to 20 MHz. The E4980A offers C (capacitance)-D (dissipation factor) measurement with a basic accuracy of ± 0.05% (C), ± 0.0005 (D) at all frequencies.

The 16451 assembly is a test fixture for measuring disc and film dielectric materials when connected to Agilent's LCR meters or impedance analyzers, and is usable up to 15 MHz as shown in Figure 2.11, can avoid the stray capacitance at the edge of the electrode and measure capacitance accurately. For permittivity measurement using the Agilent E4980A LCR meter with option 001, all PMMA and MWNT/PMMA nanocomposites samples were cut to approximately 30 × 30 × 1 mm^3 with smooth and parallel surfaces. The thickness of the samples was 200 μm.

Figure 2.12: Dielectric measurement set-up (conductivity, Loss factor, etc)

All samples were cleaned with ethanol before permittivity measurement to remove surface contaminants. However, it was found that conductive coating is necessary for permittivity measurement of all samples. A silver paint, which can dry quickly at room temperature but requires 20 hr for curing to obtain excellent electrical properties, was used to coat samples measured at room temperature by the LCR meter, which is attached with dielectric test fixture applying guarded electrode D. Before silver painting, all the samples were cleaned by wiping with a little ethanol. The Dielectric measurement is carried out from Department of physics, University of Rajasthan, Jaipur.

2.4.10 Raman spectroscopy

Raman spectroscopy is a light scattering technique, and can be thought of in its simplest form as a process where a photon of light interacts with a sample to produce scattered radiation of different wavelengths. When monochromatic radiation is incident upon a sample then this light will interact with the sample in some fashion. It may be reflected, absorbed or scattered in some manner. It is the scattering of the radiation that occurs which can tell the Raman spectroscopic something of the samples molecular structure. If the frequency (wavelength) of the scattered radiation is analyzed, not only is the incident radiation wavelength seen (Rayleigh scattering) but also, a small amount of radiation that is scattered at some different wavelength (Stokes and Anti-Stokes Raman scattering). It is the change in wavelength of the scattered photon which provides the chemical and structural information.

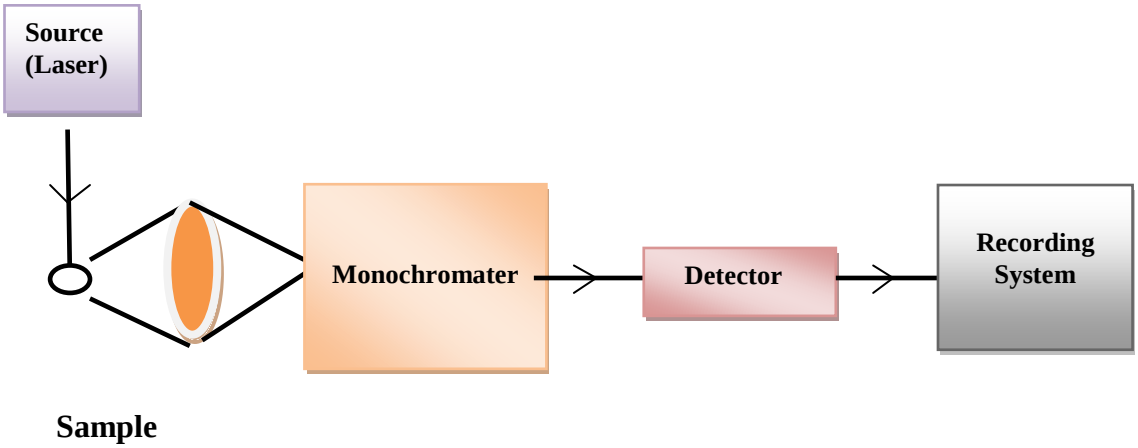

Figure 2.13: block diagram of Raman spectrosopy

2.4.11 Doppler broadening spectroscopy

In the experiment, a High Purity Germanium (HPGe) detector was used to measure the Doppler broadening spectrum. The DBS system consist of a high purity germanium detector with energy resolution of about 1.64 keV (FWHM) at 1.33 MeV, which corresponds to an energy resolution of about 1.1 keV at 511 keV respectively. The positron source was shield by multilayer of led (Pb) sheet in order for all gamma rays to annihilate in the same material. The block diagram of DBS is shown in Figure 2.14. The distance from the source to the detector and the presence of other sources was dependent on the type of experiment being performed**.** DBS measurements have been carried out using at the Department of Physics, University of Rajasthan, Jaipur. Experimental setup of DBS is shown in Figure 2.15.

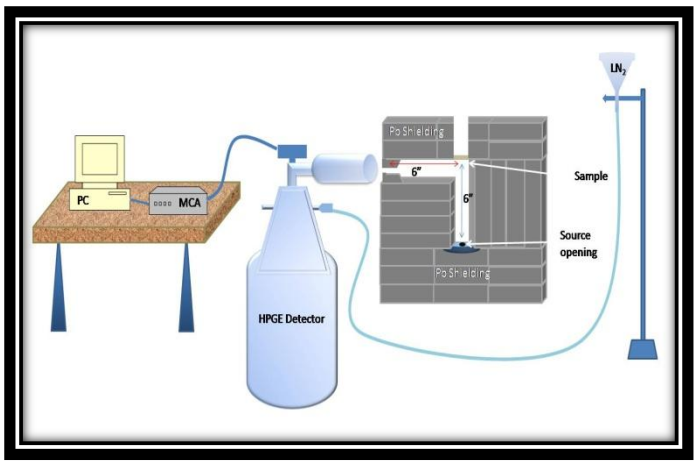

Figure 2.14: Block diagram of Doppler Broadening Spectroscopy.

Figure 2.15: Experimental setup of Doppler Broadening Spectroscopy

2.5 Data analysis

Whilst it is possible to examine the complete spectrum from a germanium detector, in Doppler broadening spectroscopy it is usual to define basic single-value parameters which describe the shape of the peak. The most common of these are known as S- and W- parameters, which are defined as the number of γ-photon counts in a pre-defined energy window over the total number of counts in the photopeak. The S-parameter is a quantitative measure of the fraction of counts in the centre of the peak, while the W- parameter measures the fraction of counts in the two wings of the peak (Figure 2.16). The exact windows used to define the S- and W- parameters will vary depending on equipment, personal preference and the aim of the experiment. In order to introduce consistency, and allow comparison of results, most measured S- and W-values have absolute values of approximately 0.5 and 0.03, respectively, but are usually quoted in relation to a reference material, usually epitaxially grown silicon [46].

The magnitude of S- (and W-) parameter depends on the size of the vacancy defect The W-parameter is more sensitive to the chemical surrounding of the annihilation site than the S- parameter, because the core electrons having a high momentum are contributing mainly in the region of large energy deviations from the annihilation energy of 511 keV.

The central parameter S-parameter is defined as ration of the counts in the central region of the annihilation line to the total number of the counts in the line. In the same way, the wing parameter W-parameter is the relative fraction of the counts in the wing regions of the line. Due to their low momentum, the annihilations with valence electron fall predominantly in the region of S- parameter. Mainly core electrons have momentum values high enough to contribute to the W parameter, respectively. In order to get maximum information out of the parameters, proper choice of the energy windows is important. The central window for S-parameter is chosen so that it covers about 50% of the total peak (S~0.5). The W-parameter window should be far enough from the peak to ensure that mainly core annihilations are accepted [47].

$$S_{parameter} = \frac{S_{region}}{T} \tag{2.2}$$

$$W_{parameter} = \frac{W_{1+}W_2}{T} \tag{2.3}$$

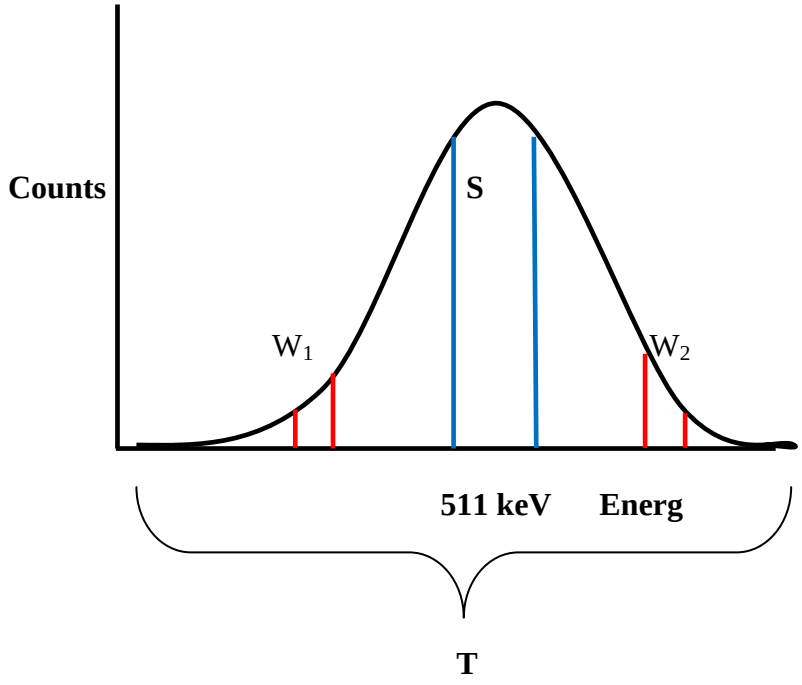

Figure 2.16: Schematic representation of S- and W- parameter region

3.1 Introduction

Fractional free volume is important in understanding gas transport through polymeric films. The amount and distribution of fractional free volume will dictate how gaseous molecules will be transported through the material. So, the free volume will determine the usefulness of a polymer for a barrier or membrane application. A polymer's free volume is the difference between the specific polymer volume in the glassy or rubbery states and the volume associated with a crystalline solid at the same temperature. Molecular chain motions and chemical structure will affect fractional free volume and its distribution within a polymer. Free volume and free volume distribution have long been used to explain differences in the gas transport properties of polymeric materials. However, only a few experimental techniques allow a comprehensive evaluation of polymeric void space. Overall, this study will allow for the direct correlation of structural chemical changes in a polymer with its effect on free volume. Positron annihilation spectroscopy (PAS) is a sensitive probe for studying defects in solids. The method relies on the propensity of positrons to become localized at open-volume regions f a solid and the emission of annihilation gamma rays that escape the system without any interaction. These gamma quanta hold information about the electronic environment around the annihilation site [48-50].

The positrons are emitted from a radioactive source to a solid. The most common source is ^{22}Na, for which the maximum energy of the emitted positrons is 0.54 MeV. Therefore the penetration depth is sufficient to probe the bulk. The positron slows down and thermalizes in the solid within a few picoseconds. After diffusing around the lattice, the thermalized positron annihilates with an electron creating two gamma quanta of energies of 511 keV, which is equivalent to the rest mass of the particles. The two quanta are emitted at approximately opposite directions. The deviation from 180° is caused by the momentum of the electron, since the momentum of the positron is negligible due to thermalization. In the case of core electrons the momentum is large while for the valence electrons it is small.

Several observables are employed in PAS to characterize defects: positron lifetime, two-dimensional angular correlation radiation (2D-ACAR), and Doppler broadening. Positron lifetime experiments are capable of distinguishing different kinds of defects but provide no direct information on chemical variations [51]. 2D-ACAR data allow the characterization of defects through the analysis of the momentum distribution of conduction- and valence-band electrons in the perturbing fields of defects, which requires detailed calculations of positron wave functions and the electronic band structure. Doppler broadening of annihilation radiation provides a sensitive method of defect characterization by measuring the momentum distribution of the electrons [52].

The principle of the method lies in the analysis of the positron annihilation line shape, which directly corresponds to the distribution of momentum of electron-positron pairs. The momentum itself is measured from the amount of the Doppler shift of the emitted photons. Because the positrons are thermalized, the total energy of the annihilation gamma rays is given by $2m_oc^2 - E_B$, where m_oc^2 is the electron rest mass energy and E_B is the electron binding energy. When there is a net center of mass energy associated with the annihilating pair, this total energy is not split equally among the two gamma rays. One gamma ray is upshifted while the other is downshifted from the center energy of $m_oc^2 - \frac{E_B}{2}$ by an amount given by $\Delta E = \frac{p_L c}{2}$ where p_L is the longitudinal component of the electron-positron momentum along the direction of the gamma ray emission. Since the direction of the gamma ray emission is random, a detector located in a given direction will record both up shifted and downshifted gamma rays. This produces an overall Doppler broadening of the annihilation peak.

In a solid, positrons predominately annihilate with outer electrons from conduction and valence bands. The analysis of the low probability events occurring from annihilation with the core electrons is not feasible in a traditional, single-detector Doppler-broadening setup due to the high level of the background. This difficulty can be overcome in a two-detector system detecting both annihilation photons and selecting only simultaneous events, thus eliminating random background counts.

3.2 Experimental Methods

Doppler broadened spectroscopy (DBS) is the principal technique used to analyze the samples described in this report. The technique examines the Doppler shift in the energy of the gamma radiation resulting from positron annihilation, which is linked to the momentum of the annihilating electrons, and thus a property of the material in which annihilation occurs. The distribution of electron momentum is expressed in the observed γ spectrum as a Gaussian-like broadening of the 511keV photo peak. Typically millions of photons would be measured, and peaks would be 10's of KeV in width, however exact measurements are dependent on the material, and the key measurement of positron annihilation spectroscopy. The energy broadening of the annihilation line described above is measured by a high-resolution energy-dispersive detector system. Liquid-nitrogen-cooled pure Ge crystals of high efficiency (about 20 %) are used. Under the applied high voltage of several kV, the annihilation photons cause a charge separation that is converted by a preamplifier into an electrical pulse. Its amplitude is a measure of the photon energy and can be registered after main amplification in a multichannel analyzer (MCA). A digital peak-stabilizing system as part of the MCA allows the long-term collection of several million counts.

The broadening of the distribution is dependent on the type of electron with which the positron annihilates. If annihilating in bulk material, it is possible that the annihilation will occur with an energetic core electron from a bulk atom. The higher momentum will cause a wider broadening of the spectrum, in comparison to a positron trapped at a vacancy defect where annihilation with a lower-momentum valence or conduction electron is more likely. Generally, the larger the defect, the lower the mean momentum of the annihilating electron, the less pronounced the broadening, and the sharper the peak.

3.3 DBS measurements

The DBS measurement of the sample MWNT/PMMA nanocomposites were taken at Thin film and membrane science laboratory, University of Rajasthan, Jaipur. The details of Doppler Broadening Spectroscopy are given in Chapter 2.

3.4 Data analysis

The DBS spectra of all the samples were recorded for 4×10^6 total counts and under the same experimental conditions. The DBS spectra of doped and pure PMMA samples are shown in Figure3.2, and 3.3 respectively. Whilst it is possible to examine the complete spectrum from a germanium detector, in Doppler broadening spectroscopy it is usual to define basic single-value parameters which describe the shape of the peak. The most common of these are known as S- and W- parameters, which are defined as the number of γ-photon counts in a pre-defined energy window over the total number of counts in the photo peak. The S- parameter is a quantitative measure of the fraction of counts in the centre of the peak, while the W- parameter measures the fraction of counts in the two wings of the peak. The exact windows used to define the S- and W- parameters will vary depending on equipment, personal preference and the aim of the experiment. In order to introduce consistency, and allow comparison of results, most measured S and W values have absolute values of approximately 0.5 and 0.03, respectively, but are usually quoted inrelation to a reference material, usually epitaxially grown silicon. The magnitude of S- (and W-) parameter depends on the size of the porosity.

3.5 Experimental results

Figure 3.1 and 3.2 show the DBAR spectrum for pure PMMA and for MWNT/PMMA. Figure 3 (a and b) shows the calculated values of the S- and W-parameters as a function of the MWNT concentration on PMMA. It is found that the S- parameter decreases with increasing the MWNT concentration that is due to decreasing the positronium fraction corresponding to decreasing the o-Ps intensity. On the other hand, the increase in the W parameter is due to increasing of positrons

annihilate at the MWNT. With increasing MWNT content, the interfacial area between MWNTs and PMMA matrix increase rapidely, which bring about increase in W-parameter. In addition, according to report by Seman et al [29], when the diameter of filled particles is in nanometer scale, nanofillers will result in the increase of W-parameter.

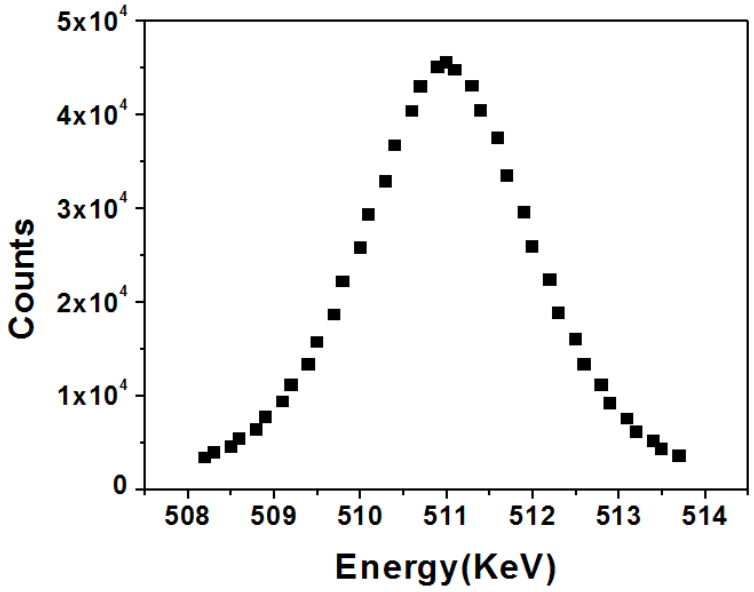

Figure 3.1: DBS spectra of pure PMMA

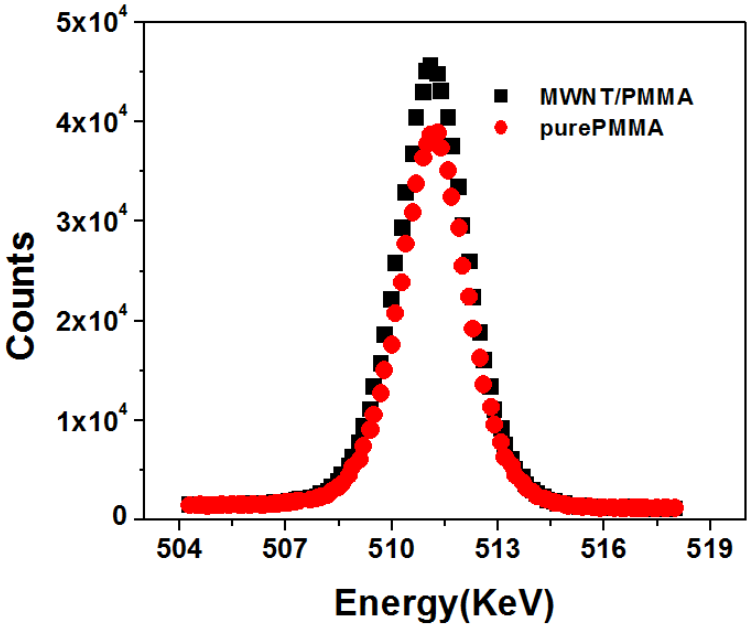

Figure 3.2: DBS spectra of Pure PMMA and MWNT/PMMA composite

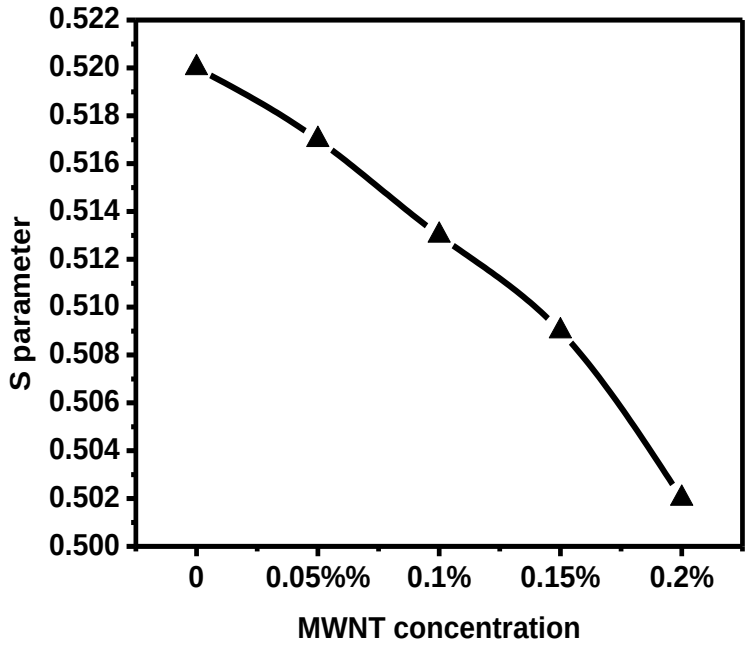

Figure 3.3(a): S- parameter as a function of the MWNT concentration on PMMA

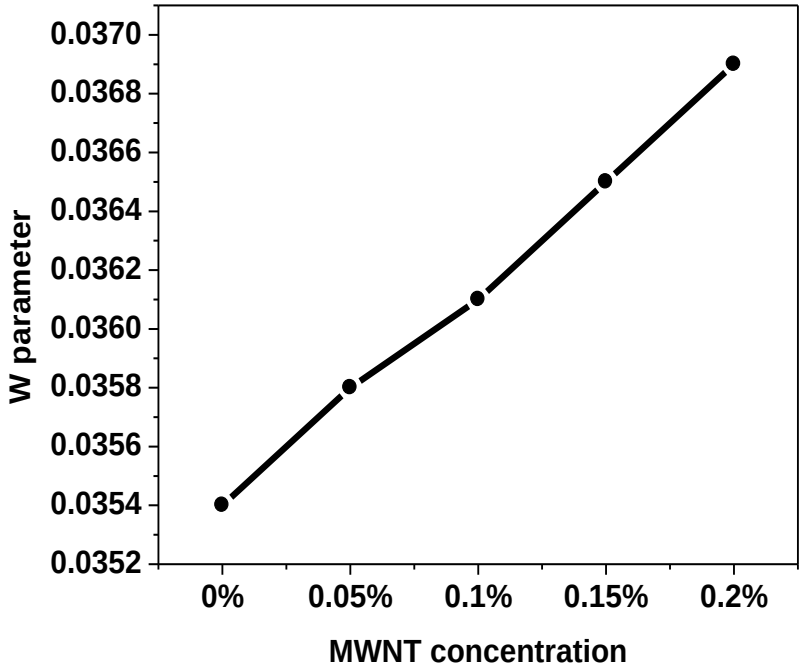

Figure 3.3(b): W- parameter as a function of the MWNT concentration on PMMA

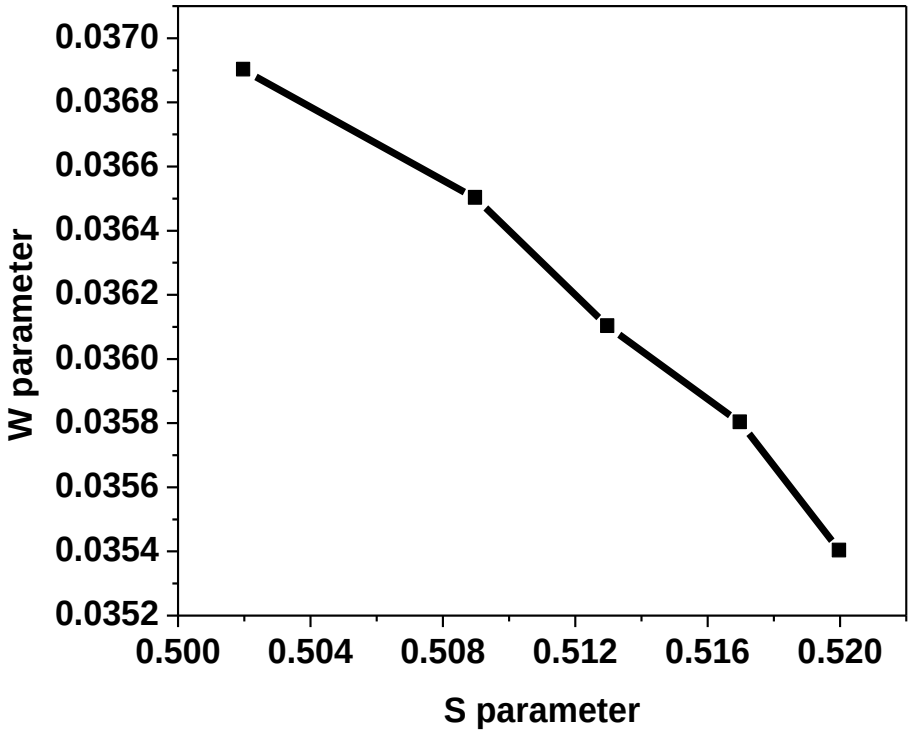

Figure 3.4: plot of W- parameter with S- parameter for the studied sample

The S-W plot for pure and doped PMMA with different concentrations of MWNT is shown in Figure 3.5. Polymers usually have poor resistance to abrasive sliding attack because of their relatively low levels of hardness and strength, high plasticity, and low thermal conductivity. Fillers will certainly improve these properties therefore promote the hardness. The mechanisms revealing how fillers improve hardness are not well established. There appear to be two broad explanations. One of them stems from the observation that excess filler concentration is noticed on the composite surface after prolonged sliding. Based on this observation the bulk of the load is supported by the concentrated filler resulting in increased hardness of the composite. The second suggestion is that fillers may improve the adhesion of the transfer film to the counter face and thereby suppress the hardness. While the first explanation might be accepted easily by common sense, the second is complicated. it is considered to be either physical or chemical in nature. Physical interaction involves

Vander Waals forces and is comparable in strength with the forces between molecular chains within the polymer itself.

Increasing the MWNT concentration on PMMA leads to increase the hardness and increase the W parameter as a result of increasing the chemical composite in the samples (increasing the positron annihilating at MWNT). This correlation also has two different slopes that depend on the hardness of the samples (i.e., MWNT concentration on PMMA). Figure 3.5 (a) shows the S- parameter as a function of wt% of MWNT. The pure polymer has an S value of 0.5232, with an experimental error of 0.0011. For all fillers S decreases with increasing wt% of MWNT. This is mainly due to a decrease in positronium formation. The S- and W- parameters can both be described as a linear combination of the bulk- and defect-related sites. The S-parameter reflects the annihilation probability of positron with the low-momentum valence electrons. Therefore, it suggests that the main origin of a decrease in S-parameter is due to a decrease in the relative concentration of defects evolution can be obtained in both DBS measurement. Positron annihilation correlation plots of the S-parameter and its complementary W-parameter are found to be useful in distinguishing various defect spices or the chemical surrounding of the defects. It can be seen in Figure.3.6 the data point fall on a straight line, suggesting that the defect specie do not change with MWNT doping.

3.3 Conclusion

In this chapter, the Doppler broadening of annihilation radiation in PMMA/MWNT has been studied using ^{22}Na as a positron source. MWNT/PMMA nanocomposites membranes have been prepared by dispersing different concentrations (wt% - 0.05, 0.1, 0.15 and 0.2%) of multiwall carbon nanotubes (MWNT) in Poly methyl methacrylate (PMMA) matrix using benzene as a solvent. Fractional free volume is important in understanding gas transport through polymeric films. A polymer free volume is the difference between the specific polymer volume in the glassy or rubbery state and the volume associated with the crystalline solid at the same temperature. Doppler broadening of annihilation radiation offer a sensitive method of defect characterization by measurement the momentum distribution

technique. Doppler broadening spectrum technique is useful to define basic single value parameters which describe the shape of the peak.

The S- parameter and W- parameter were measured from the spectrum of different sample as a function of the relative weight. From this experiment we find out the behavior of the S- parameter and W- parameter in terms of positron annihilation and positronium formation for the various samples. Doppler broadening spectroscopy is direct correlate between these parameter and the various physical characteristics of Carbon nanotube.

4.1. Introduction

Due to their novel properties, both single-walled and multi-walled carbon nanotubes (CNTs) are considered potential candidates as filler materials for polymer composites with enhanced mechanical, electrical, thermal, and/or optical properties. The issues related to dispersion of CNTs in the polymer matrix and the formation of strong polymer/CNT interface for effective load transfer necessitate CNT surface modification.

The following tasks were be conducted,

a) Confirmation of MWNT on PMMA matrix by XRD
b) Orientation study of MWNT/PMMA nanocomposites by Raman spectroscopy and FT-IR spectroscopy
c) Study the effect of MWNT dispersion on morphology.
d) Study the effect of MWNT concentration on I-V characterics.
e) Measure the refractive index of the prepared MWNT/PMMA nanocomposites.
f) Study the optical properties of MWNT/PMMA nanocomposites

Most of the nanoparticles are introduced in to host matrixes to improve various properties [53,54]. Among various nanoparticles, carbon nanotubes are the ideal candidate because of their intrinsic properties such as high aspect ratio, (length to diameter ratio) and nanocsale diameter. The orientation of carbon nanotube in polymer is very difficult because carbon nanotube existence of high vanderwaals interaction between nanotubes. Orientation of the carbon nanotube in polymer matrix is one of the important tasks. Well dispersion carbon nanotube in polymer matrix can enhance the properties of the nanocomposites [55]. A good dispersion may be achieved by surface modification of the nanoparticles under appropriate condition. Carbon nanotube not only tend to agglomerate, but are often prepared in bundle-like structure. In order to take advantage of their high surface area for interacting with the polymer, the bundle has to be separated into individual nanotubes. For MWNT this can usually do by ultrasonication. Any agglomerations of the fillers reduces the interfacial area in the composition and reduce the opportunity to take advantage of the

unique nanofiller properties. The preparation method of MWNT/PMMA composites is described in Chapter 2.

In nanocomposites the charge carriers formed by doping conducting particles and dominates the electronic properties and better understand of the charge transport is very important task. The charge carriers generated in the process of doping in polymers. High aspect ratio of carbon nanotube leads to percolation at low loading [56,57]. Alignment has also been found to improve conductivity. The properties of these nanocomposites depend on the composition, concentration, particle size and dispersion homogeneity. X-ray diffraction has played a central role in identifying and characterizing solids since the early part of the century. X-ray diffraction is a useful tool to obtain structural information [58].

UV-VIS spectroscopy is used to study the change in the optical properties of polymers and polymers nanocomposites. Four Transform Infrared Spectroscopy (FTIR) has been recognized as a powerful tool for elucidation of structural information, the position, intensity and shape of vibrational bands, useful in clarifying conformational and environmental changes of polymer at the molecular level. These composite membranes have also been characterized by Raman spectroscopy, optical micrograph and electrical measurement. Raman spectroscopy is one of the technique for confirmation of the presence as well as alignment of the carbon nanotube [59].

Most of the polymers have refractive index in the range 1.35-1.5. For optical applications polymer with higher refractive index are required. In the last years, the polymer doped with metal oxide nanoparticles have been studied as alternative material for optical application [60,61].

4.2 Result and discussion

4.2.1 X-ray diffraction (XRD)

The Figure 4.1 shows typical X-ray diffraction patterns for MWNT/PMMA composites. These diffraction patterns exhibit the peaks at 2θ = 15.3°, 20.5° and 25.2°. In additional, in comparison to the pure PMMA a new peak at 2θ = 43.5° has

also been observed corresponding to the graphite like diffraction comes from the presence of MWNT and small amounts of catalytic particles encapsulated inside the walls of carbon nanotubes within composites.

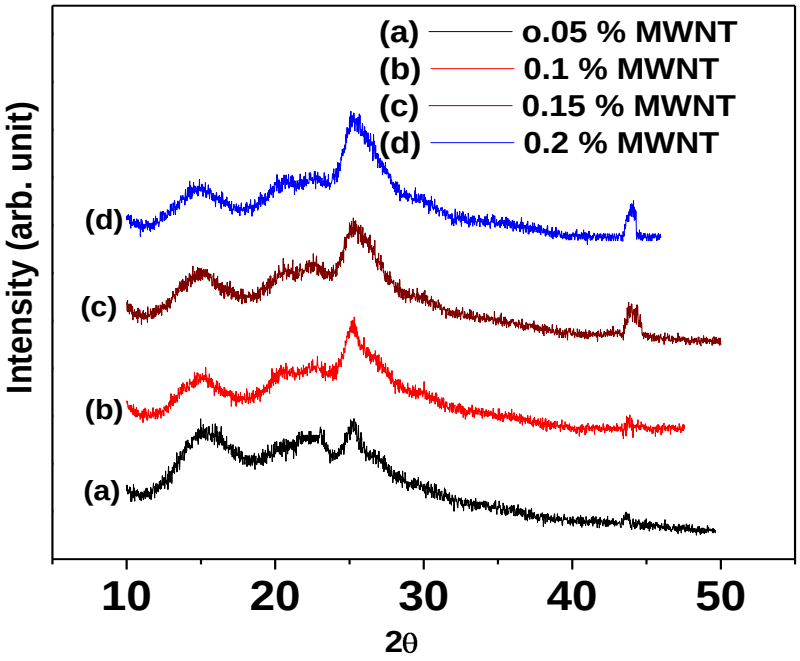

Figure 4.1: XRD pattern of MWNT/PMMA nanocomposites

The XRD pattern of MWNT/PMMA composites indicate that axis of the MWNT, and thus the percentage crystallinity of the outer layer of the intensity of crystalline peaks (25.2° and 43.5°) increased with the increasing concentration of MWNT in composites. This may be attributed to that the excess of MWNT in PMMA matrix creates extended microcrystalline domains in the composites and hence the corresponding peak intensity is increased. In other words, during the polymerization an amorphous layer of PMMA is coated on the surface of the MWNT, therefore the MWNT easily orders the PMMA macromolecule along the tubular composite increases. These dominant features indicate that the formation and stability of the new structures is enhanced when MWNT is combined with PMMA.

4.2.2 Optical micrograph

The image for all samples is shown in Figure 4.2. It is clear from the Figure 4.2 that at low concentration (0.05% and 0.1%), MWNT uniformly distributed within the polymer matrix without forming any significant amount of agglomerates up to a MWNT concentration of 0.1% as shown in Figure 4.2 (b & c). But when the dopaint concentration increase further it leads to aggregation of MWNT in PMMA matrix as shown in Figure 4.2 (d & e).

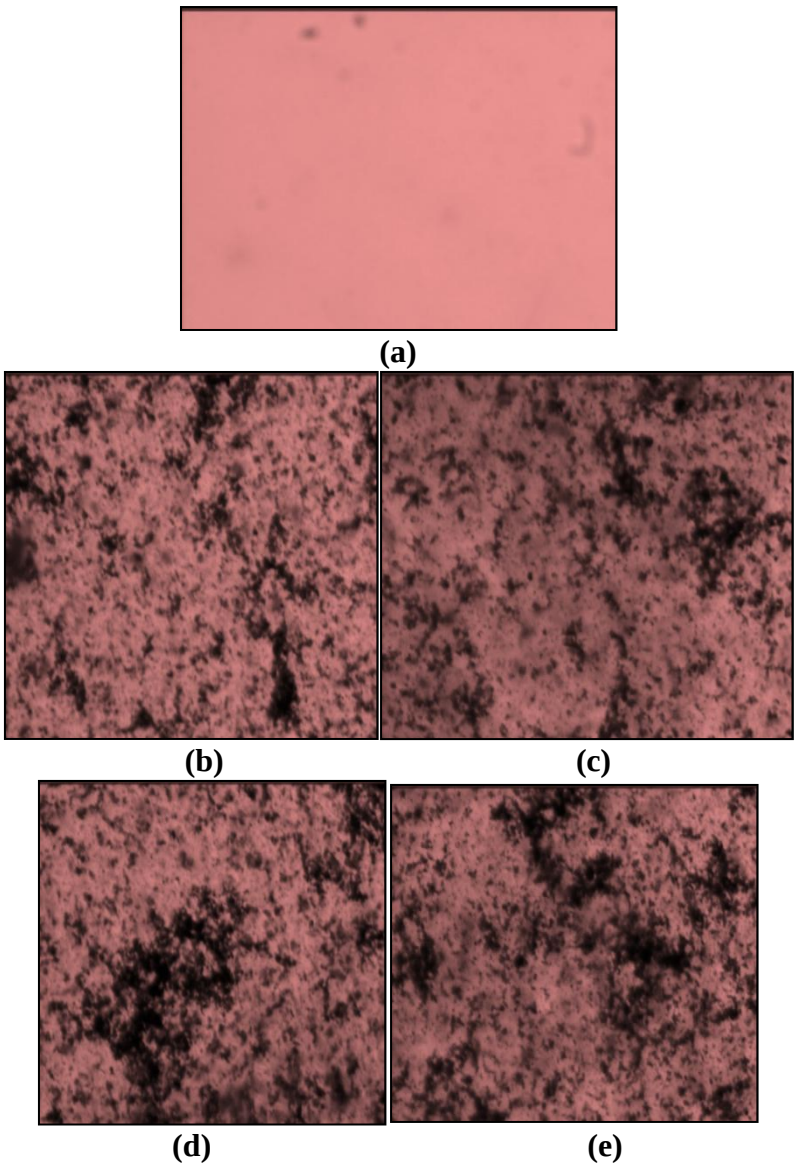

Figure4.2: Optical microscope images of the nanocomposites,(a)Pristine PMMA (b)MWNT (0.05%), (c)MWNT (0.1%), (d)MWNT (0.15%), (e)MWNT (0.2%)

4.2.3 Raman spectroscopic measurement

Raman spectroscopy is one of the technique for confirmation of the presence of the carbon nanotube in polymer matrix. The Raman spectroscopic measurements show the characteristic peaks at 981, 1449, 1727 and cm^{-1} which corresponds to pure PMMA and the peak at 1333, 1587 cm^{-1} corresponds to the MWNT as shown in the Figure 4.3.

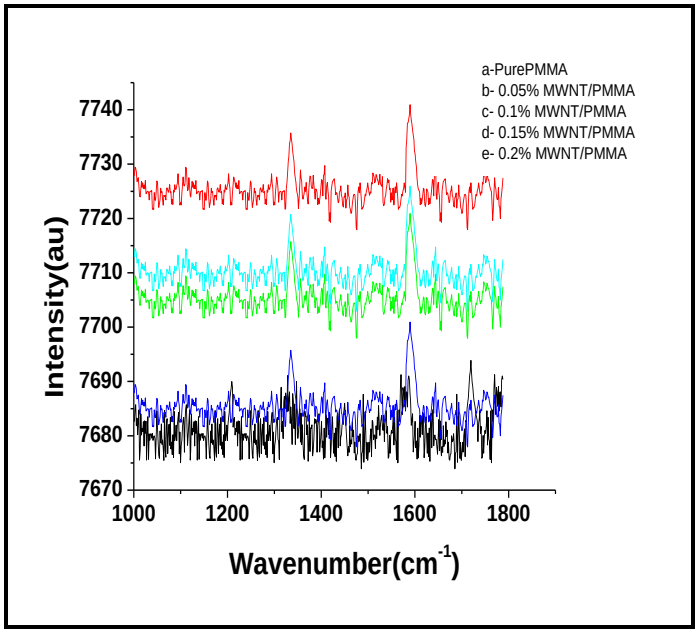

Figure 4.3: show the Raman spectra of pure PMMA and MWNT/PMMA nanocomposites

The Figure 4.3 shows Raman spectra of pure PMMA and dispersed MWNT in PMMA matrix. These spectra revealed that the presence of MWNT in polymer matrix is confirmed by identifying the peaks at 1333 and 1583 cm^{-1} corresponding to the D-band and G-band respectively. The G-band near the 1583 cm^{-1} may attribute to a splitting of vibration mode of graphite carbon in MWNT. Raman spectroscopy is a powerful tool to investigate the presence and characteristics of CNT in a sample. In Figure 2 we can observe the D- band at the raman shift of 1339 cm^{-1} and G- band at 1587cm^{-1} both these features are features of graphite. G- band is the characteristics of graphitic phase corresponding to in plain vibration of C atoms which indicates the

presence of crystalline graphitic carbon in MWNTs [62]. D- band has been attributed to disorder induced features such as defects generated in the grapatic planes of MWNTs due to presence of amorphous defects in graphitic structure.

The Raman spectra for higher wt% of MWNT in polymer matrix indicated the sharp increase in peak intensity and the peak positions slightly shift toward lower wave number side. These effects are attributed to the higher wt% of MWNT which create principal homogeneous optical channels within polymer composite. These measurements clearly reveal that the Raman intensity is sensitive to the degree of orientation of MWNT within polymer matrix.

4.2.4 UV-Visible spectroscopy

Optical measurements of MWNT/PMMA nanocomposites are characterized by UV-VIS spectrometer. FIgure.4.4 shown the transmission spectra of MWNT/ PMMA nanocomposites in wavelength range 300-900nm. From this Figure (Figure 4.4) we show that the transmittance intensity decreases with increasing of MWNT wt%. The reason for this behavior is that the increase in wt% of MWNT, increase the density of nanocomposites state, which reduce the transmittance value. It is noticed that these nanocomposites have higher transmission value in the visible range of spectrum.

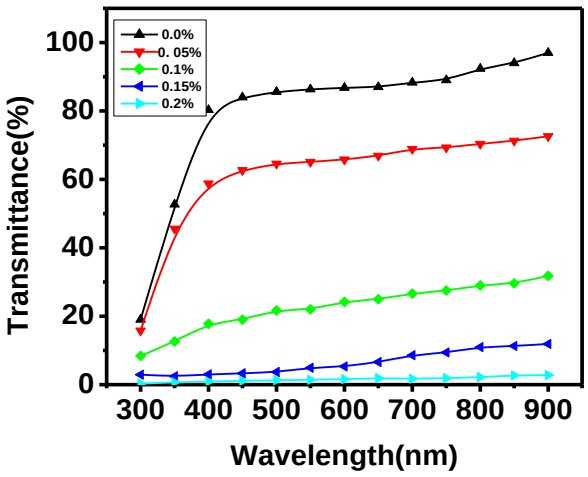

Figure 4.4: Transmission spectrum of PMMA and MWNT/PMMA nanocomposites

The optical energy band gap of these nanocomposites were calculated using the Tauc's relation [63]

Given by:

$$\alpha(h\nu) = B(h\nu - E_g) \quad (4.1)$$

where B is a constant. hν is the photon energy, E_g is the optical band gap and α is the absorbtion coefficient. Thus the optical energy band gap of the nanocomposites was determined by plotting $(\alpha h\nu)^2$ verses photon energy(hν), and by extrapolating the curve to αhν=0 as shown in Figure 4.5.

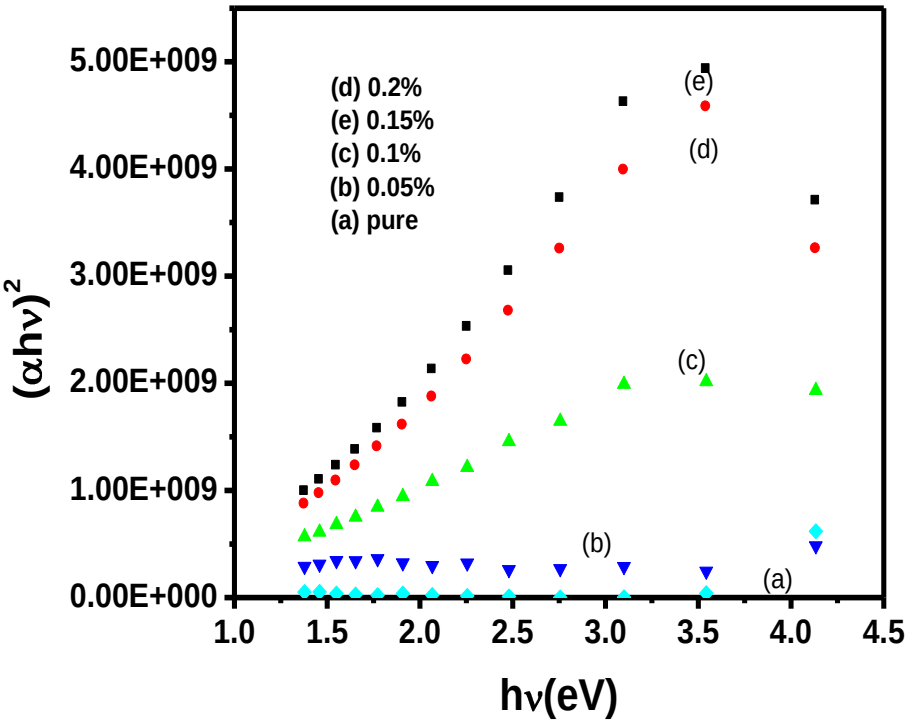

Figure 4.5: Optical energy band gap of PMMA and MWNT/PMMA nanocomposites

The absorption coefficient (α) of the MWNT/polymer nanocomposites was determined from transmittance measurement. The calculation of absorption coefficient (α) of these nanocompoites in this range was calculated using following expression. The absorption coefficient (α) is given by [64]

$$\alpha \geq \frac{1}{d} \ln \frac{1}{T} \qquad (4.1)$$

Where d is the sample thickness and T the transmittance.

Table 1 show the energy band gap of MWNT/PMMA nanocomposites. The value of optical energy band gap found to be decreasing from 4.13 to 2.4 eV as the concentration of MWNT increase from 0.05% to 0.2%. In general, the density of localized state in the nanocomposites increases with the MWNT concentration which leads to decrease in the band gap.

Table 1 The energy band gap of MWNT/PMMA nanocomposites

MWNT/PMMA	0.0wt%	0.05wt%	0.1wt%	0.15%	0.2wt%
Eg (eV)	4.13	3.54	3.1	2.48	2.4

4.2.5 SEM (scanning electron microscope)

The surface morphology of pure MWNT/PMMA nanocomposite is determined by scanning electron microscopy. As shown in Figure.4.6 (a), the SEM image for 0.05% MWNT /PANI composite reveal that the MWNTs are well distributed within PMMA matrix and that most of the MWNTs are in the form of small bundles or single tubes covered by the large amorphous clusters of PMMA. It is found that at low loading in PMMA matrix oriented well while MWNTs at higher loadings in PMMA matrix agglomerate.

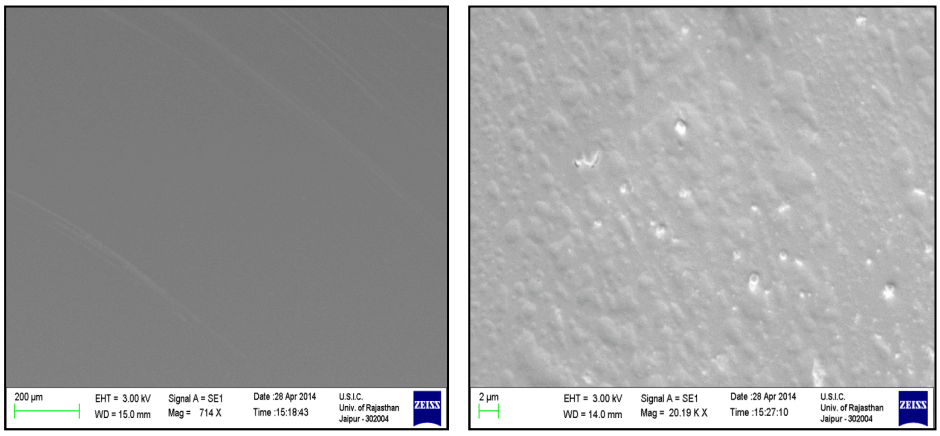

(a) (b)

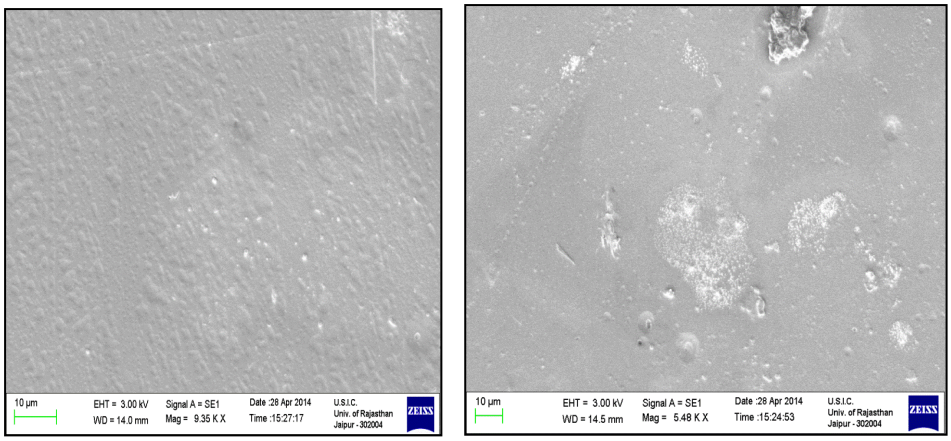

(c) (d)

Figure 4.6: SEM images for (a)pure PMMA (b) 0.05%% MWNT/PMMA composite, (c) 0.1% MWNT/PMMA composite and (d) 0.2% MWNT/PMMA composites

4.2.6 FTIR spectroscopy

The FT-IR spectra of MWNT/PMMA nanocomposites are shown in Figure4.7 (a) and (b). The C=O stretching vibration of the PMMA macromolecules in the respective composite is found at 1730cm^{-1}. The peak at 1384-1464 cm^{-1} are the bending vibration of CH_2 and CH_3 group and peaks at 1000-1260 cm^{-1} are due to the strerching vibration of the C-O-C group of the infiltrated PMMA. The band from 950-650 cm^{-1} is due to the bending of C-H. The broad absorbtion region ranging from 3100-2900 cm^{-1} can be assigned to the stretching vibration of C-H.

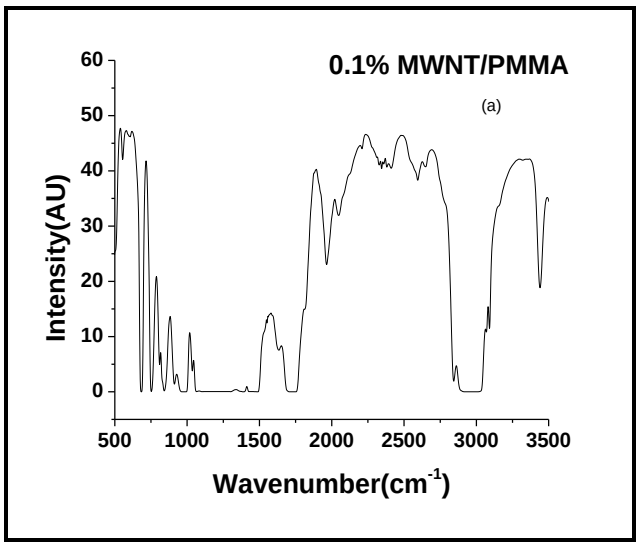

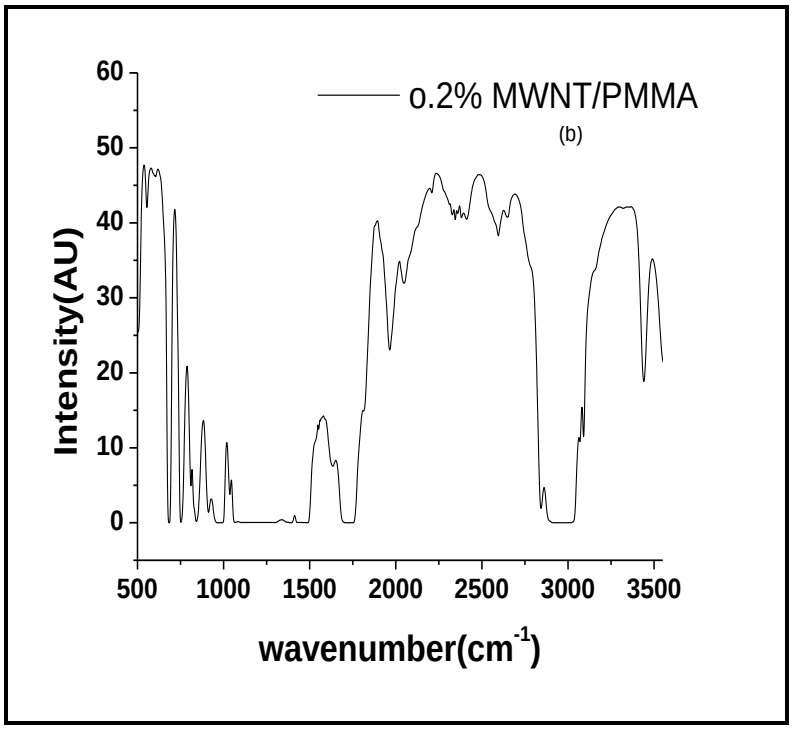

Figure 4.7 FT-IR spectra of MWNT/PMMA nanocomposites (a) and (b)

4.2.7 I-V characteristics

The Figure 4.8 shows I-V characteristics of MWNT/PMMA nanocomposites. The electrical conduction behavior of these nanocomposites is measured by a two probe method at room temperature. We have measured electrical conductivity of different MWNT doping concentration in PMMA matrix. It is found that the conductivity measured in these MWNT/PMMA nanocomposites membranes is giving dramatically difference which is depends upon MWNT concentration in PMMA matrix. At low concentrations with the increase of MWNT content, the current is almost linearly dependent in volt and the conductor sites increase in PMMA matrix for electron hopping mechanism and increase of conductivity is impeded by increase of MWNT content. At high concentration, the current is a function of applied voltage and this dependency of current in voltage can be understood as a semiconducting behavior. After this content of MWNT the Vanderwalls interaction causes agglomeration of CNTs and leads to decrease conductivity.

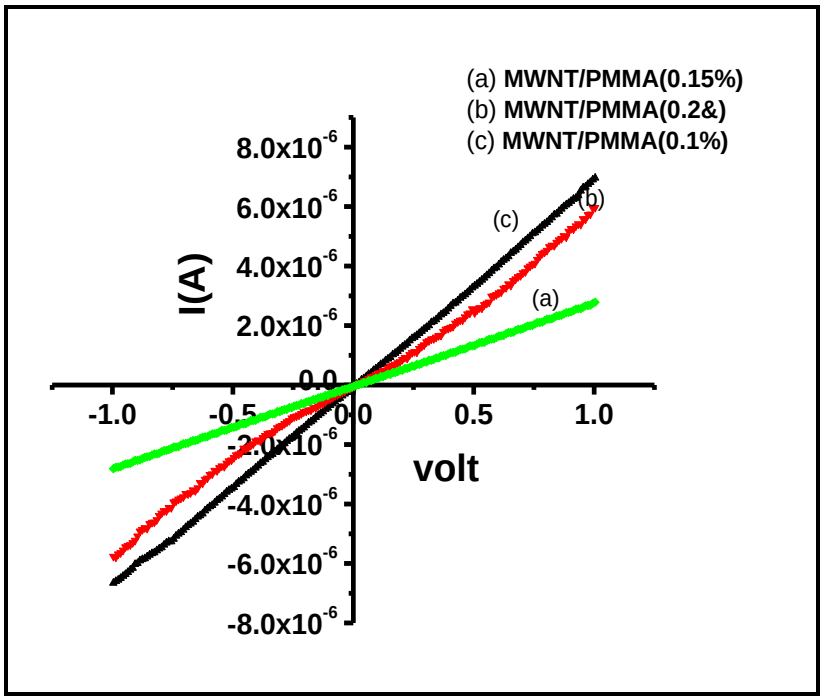

Figure 4.8: I-V characteristics of MWNT/PMMA nanocomposites

In fact, this I-V characteristic is a compromise between electron hopping effect and agglomeration of CNTs that is a consequence of increasing of MWNT content. From Figure 4.8 it is clear that the I-V characteristics of these nanocomposites is like as a semiconductor so we can say that MWNT/PMMA nanocomposite behave like as semiconducting material.

4.2.8 Refractive Index

The dependence of refractive index on the MWNT wt% in PMMA matrix is shown in Figure 4.9. The refractive indexes of MWNT/PMMA nanocomposites were determined from ellipsometric data. It is concluded from Figure.4.9 that refractive index is found to be increase with increase MWNT concentration in PMMA matrix. The refractive index of MWNT is approximately 1.55. This behavior can be understood as, at starting MWNT/PMMA nanocomposite is in dilute form, after this concentration (0.1%) MWNT disperse in PMMA matrix relative uniformly up to 0.15%, so the value of refractive index is approximately constant and after the increase dramatically.

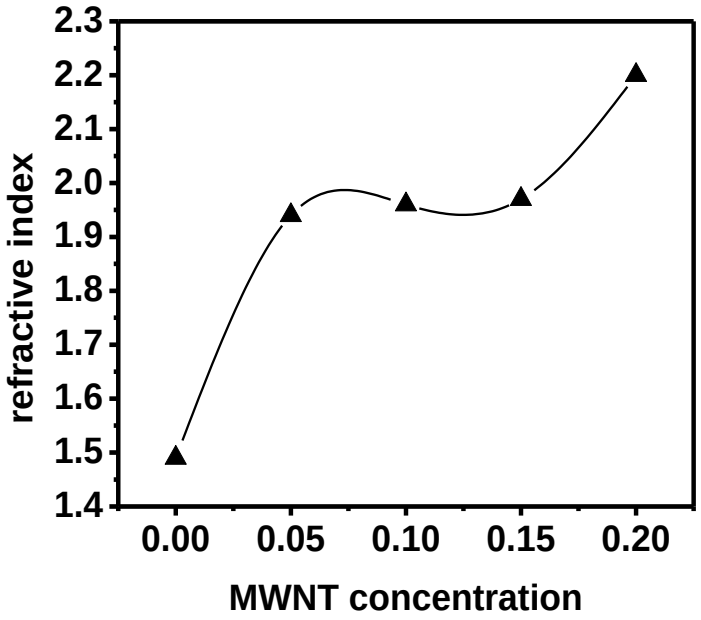

.

Figure 4.9: Refractive index of pure PMMA and MWNT/PMMA nanocomposites as a function of MWNT wt (%)

4.3 Conclusion

Chapter 4 deals with characterization of nanocomposites (wt% - 0.05, 0.1, 0.15 and 0.2) of multiwall carbon nanotubes (MWNT) in Poly methyl methacrylate (PMMA) matrix by electrical and optical properties studied at room temperature. Most of the nanoparticles are disperse into host matrixes to improve various properties. Among various nanoparticles, orientation of carbon nanotube in polymer matrix is one of the important task. Well dispersion carbon nanotube in polymer matrix can enhance the properties of the nanocomposites. X-ray diffraction is a useful tool to get structural information. In this Chapter the samples are characterized by XRD, U-V visible, Optical micrograph, FT-IR, SEM measurement, Raman spectroscopy and I-V characteristics.

It is found that the conductivity measured in these MWNT/PMMA nanocomposites membranes is giving dramatically difference which is depends upon MWNT concentration in PMMA matrix. The dielectric constant was measured via

MT-4080 Handheld precision LCR meter. Refractive index found to be increase and dielectric constant has been increased dramatically. The dispersion of the MWNT in PMMA was examined by optical microscopy and SEM measurement. UV-VIS spectra show that higher MWNTs concentration significantly decreases the transmittance of the MWNT-PMMA nanocomposites. Experimental results show here that CNT/polymer nanocomposite membranes can be used as a good charge separating media.

5.1 Introduction

A dielectric material is an electrical insulator which can be polarized by an applied electric field. When a dielectric material is placed in an electric field, electric charges do not flow through the material as they do in a conductor, but only slightly shift from their average equilibrium positions causing dielectric polarization. Because of dielectric polarization, positive charges are displaced toward the field and negative charges shift in the opposite direction. This creates an internal electric field that reduces the overall field within the dielectric itself. Dielectrics are important for explaining various phenomena in electronics, optics, and solid-state physics. Polymers have been widely used as electrical insulation materials since the early 20th century [65]. The dielectric properties of insulation polymers can be change by disperse small fillers such as carbon nanotube etc. In part of the research presented in this thesis, the dielectric properties of PMMA polymer matrix dispersed with multiwall carbon nanotube have been investigated. Polymer nanocomposites display improved dielectric, thermal and mechanical characteristics compared with pure polymers, without requiring any significant change of polymer processing [66]. Thus, nanocomposite materials are considered promising for electrical insulation in the near future. The second aspect of research presented in this thesis investigates the dielectric properties of Poly (methyl methacrylate) (PMMA) (MWNT) nanocomposites and analyzes the effect of MWNT loading.

To study the Dielectric properties of MWNT/PMMA nanocomposite, we have to measure the dielectric constant, a.c. conductivity, dielectric loss and Loss tangent. These all properties show the dielectric behavior of MWNT/PMMA nanocomposites. The dielectric behaviors of the nanocomposites were studied systematically over a range of frequencies to determine the dependence of dielectric constant, dielectric loss tangent and dielectric strength on these parameters. Conductive filler/polymer nanocomposites are important material because they show a dramatic increase in their dielectric constant close to the percolation threshold.

5.2 Theory

5.2.1 Dielectric constant

One of the important goals in nanocomposites fabrication is to enhance electric properties. The definition for dielectric constant relates to the permittivity of the material ( ) is as describe in below.

The dielectric constant is a property of an electrical insulating material, equal to the ratio of the capacitance of a capacitor filled with the given material to the capacitance of an identical capacitor in a vacuum without the dielectric material. The value of dielectric constant is expressed as-

$$\in' = Cd/\in_0 A \tag{5.1}$$

Where C is the value of capacitance of a nanocomposites, d is sample thickness and A is surface area of the sample, ε_o is the dielectric constant in vacuum and value is 8.854×10^{-12} F/m, A (effective area) $= \Pi r^2 (\mathrm{m}^2)$

Dielectric constant is a number without dimensions. It denotes a large-scale property of dielectrics without specifying the electrical behavior on the atomic scale. The value of the static dielectric constant of any material is always greater than one, its value for a vacuum. Water has a relatively high dielectric constant. Inorganic materials generally have higher dielectric constant compared to polymeric materials. Intrinsically they contain ions and polar groups which contribute to their high dielectric constant. Both dielectrics with low and high dielectric constant are very usefull in electronic industries. Low dielectric constant is required basically as insulator. Their applications ranged in isolating signal-carrying conductors from each other, fast signal propagation, interlayer dielectric to reduce the resistance-capacitance (RC) time delays, crosstalk and power dissipation in the high density and high speed integration. Dielectric materials are also employed to encapsulate the balls which bridged the die and substrate. This encapsulation is specifically called under fill which helps to protect any circuitry failures as well as reducing thermal mismatch between

the bridging layers. In LED encapsulation low dielectric materials is used for insulation at the lead frame housing [67,68].

5.2.2 A.C. conductivity

Low frequency conductivity and dielectric measurements in frequency range of 100–10^5 Hz have been investigated. This has been given additional information on conductivity mechanism that dc conductivity measurements alone do not provide. That is why this technique has been used extensively in many research areas in condensed matter physics, glass science, material science and polymer science. This is the major tool for study of ionic conduction in glasses, ceramics and in polymeric materials.

The low frequency measurements provide important information about conduction in the regime of temperature, doping, concentration and so on, where bulk dc conductivity of system is relatively low [69]. The charge transport mechanism polymers has been investigated recently using a number of experimental methods like ac conductivity, dielectric relaxation, photoconductivity etc. Dielectric spectroscopy has been found to be a valuable experimental tool for understanding phenomena of charge transport in conducting polymers [70]. Since the discovery of electrical conduction in doped polyaniline a variety of conducting conjugated polymers such as polypyrrole, poly (p-phenylene) and polyaniline have been successfully developed and put to a number of applications. AC electrical conductivity $\sigma_{ac}(\omega)$ is measured by the following equation Elliott, (1987):

$$\sigma_{ac}(\omega) = \sigma_{total}(\omega) - \sigma_{dc}(\omega) \tag{5.2}$$

Where ω is the angular frequency $(= 2\Pi f)$ $\sigma_{total}(\omega)$ is the measured total electrical conductivity $\sigma_{dc}(\omega)$ is the DC conductivity which depends strongly on temperature, it dominates at low frequencies and high temperatures, Whereas the σ_{ac} which has a weaker temperature dependence than σ_{dc} and dominates at high frequency and low temperature. The relation for the frequency dependence a.c. conductivity is given by:

$$\sigma_{ac} \quad \omega \quad = A\sigma^{s} \tag{5.3}$$

A is a constant, and (s) is a function of temperature which is determined from the slope of a plot $\ln\sigma_{ac}(\omega)$ versus $\ln(\omega)$.

The a.c. conductivity of the material is measured using a simple relation

$$\sigma_{ac} = 2\prod f \in_0 \in'' \tag{5.4}$$

Here f is the frequency of applied electric field.

5.2.3 Dielectric Loss

The dielectric loss is a measure of energy loss in the dielectric during a.c. operation, which is a material property. The permittivity of a dielectric material has both real and imaginary mathematical representations. The imaginary part of permittivity is represented in mathematical equations as ε||. This imaginary part of permittivity describes the energy loss from an a.c. signal as it passes through the dielectric. The real part of permittivity, ε_r is also called the dielectric constant and relative permittivity. The permittivity of a material describes the relationship between an a.c. signal's transmission speed and the dielectric material's capacitance [71-72]. When the word "relative" is used in front of permittivity, the implication is that the number is reported relative to the dielectric properties of a vacuum**.** Imaginary part of the dielectric permittivity which is a measure of how much field is lost as heat during the polarization of a material by an applied alternating electric field is also termed as dielectric loss [73]. The characteristic orientation of the dipoles in an electric field results in a frequency variation of dielectric constant and loss over a broad band of frequencies. The loss tangent is given as:

$$\tan\delta = \frac{\varepsilon''}{\varepsilon'} \tag{5.5}$$

5.3 Experimental

5.3.1 Dielectric spectroscopy

The capacitance and D-factor of the nanocomposites in this research with parallel plate prototype was measured by a HP 4275 Multi-Frequency LCR Meter. The measurement was conducted at middle frequency range from 100 Hz to 10^5Hz. The ε values of the nanocomposites were calculated from capacitance measurements. Dielectric constant and dielectric loss tangent $(\tan\delta)$ can be calculated from the capacitance and Dissipation factor measured by the equation which is describe in previous section.

5.4 Results and Discussion

The dielectric constant (ε'), dielectric loss (ε''), loss tangent $(\tan\delta)$, and a.c. conductivity (σ_{ac}) were evaluated using the standard relations of these parameters.

5.4.1 Dielectric Constant

In Figure 5.2 it is found that at lower frequency range the dielectric constant of pure PMMA and PMMA/MWNT composites depends on frequency and decrease with increasing frequency. Such behavior of the dielectric constant can be understood by the polarization. It is interesting to note that the dielectric constant is independent of frequency at higher frequency range for all weight fractions of PMMA/MWNT nanocomposites. It is due to the fact that the dipoles do not have sufficient time to orient themselves in the electric field direction; therefore, with the increase in frequency, the tendency for the polarization is expected to decrease, resulting in the decrease of dielectric constant [74].

Table 1: Dielectric constant for pure PMMA and PMMA/MWNT composites at 100 Hz frequency and room temperature.

MWNT Concentration (%)	Dielectric constant (ε')
0	3.6
0.05	4.46
0.1	5.13
0.15	5.37
0.2	7.28

Table 1 lists the dielectric constant of pure PMMA and PMMA/MWNT nanocomposites with MWNT contents at 100 Hz frequency. It is observed that the dielectric constant increases with increasing MWNT concentration. This interesting difference of dielectric constant of different nanocomposites can be understood by the Interfacial polarization. Interfacial polarization arises for electrically heterogeneous materials where two phases differ from each other in dielectric constant and conductivity. The interface polarization takes place when electron oriented under electric field. Finally, interfacial polarization results in an increase in the dielectric constant due to the random mobility of charge carriers which gets trapped at the interface of a multiphase material with different conductivity. The interface across the PMMA and MWNT may be a source of the large dielectric constant [75]. So increase of MWNT concentration will increase the number of interfaces, which will result in increase of the dielectric constant.

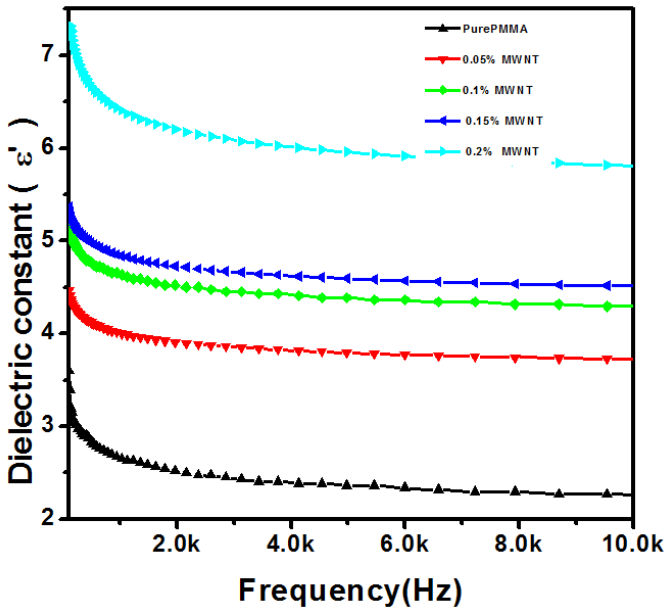

Figure 5.1: Variation in dielectric constant of PMMA and PMMA/MWNT nanocomposites.

5.4.2 Dielectric Loss

The variation of the dielectric loss of PMMA/MWNT composites as a function of frequency at room temperature is shown in Figure 5.2.

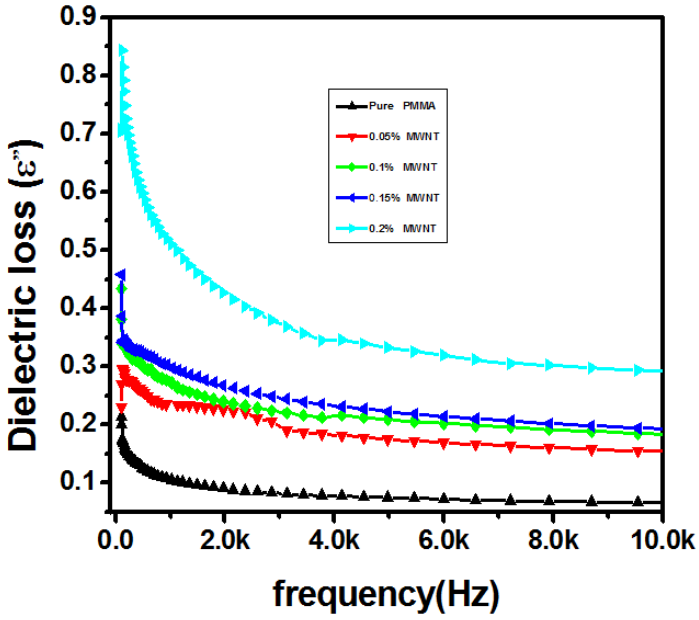

Figure 5.2: Variation of dialectic loss with frequency for (PMMA/MWNT) composites.

It is known that the loss tangent $\tan\delta$ is defined as $\frac{\varepsilon''}{\varepsilon'}$. It is interesting to note that $\tan\delta$ shows a maximum at particular frequency. There is a strong correlation between the conduction mechanism and the dielectric behavior of composites. The conduction mechanism in composites is considered as due to hopping of electron. The explanation of the occurrence of peaks in the variation of loss tangent with frequency can observed when the hopping frequency is approximately equal to that of the externally applied electric field; i.e. it means resonance phenomena [78]. The condition for observing a maximum in $\tan\delta$ of a dielectric material is given by the relaxation-

$$\omega\tau \sim 1 \qquad (5.6)$$

where $\omega = 2\Pi f_{max}$ and f_{max} proportional to the hopping probability. τ is the relaxation time.

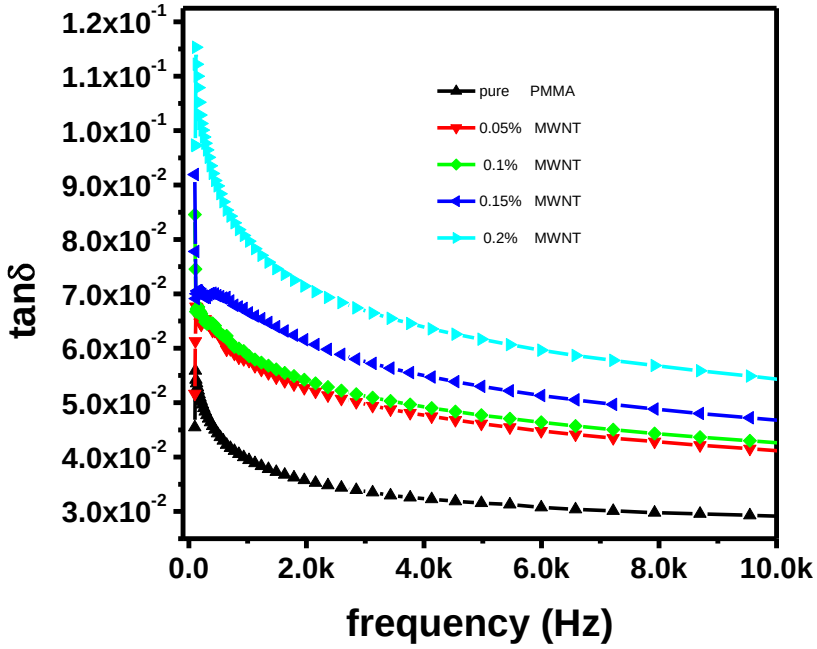

Figure 5.3: Variation of loss tangent with frequency for (PMMA/MWNT) composites.

5.3.4 A.C. conductivity

The general trend of conductivity is to increase according to increase in frequency. The variation of a.c. conductivity with different composites of PMMA/MWNT at frequency of 100 Hz at room temperature is shown in Figure 5.4. The a.c. conductivity obeys the empirical law for frequency dependence which is given by above equation 5.3 [77].

It is conclude that by incorporation of multiwall carbon nanotubes inside the PMMA matrix, there is a increase in charge transport and by heat treatment the conductive grains of MWNT expand due to which mobility of carriers increase between the grains and hence ac conductivity increase [78].

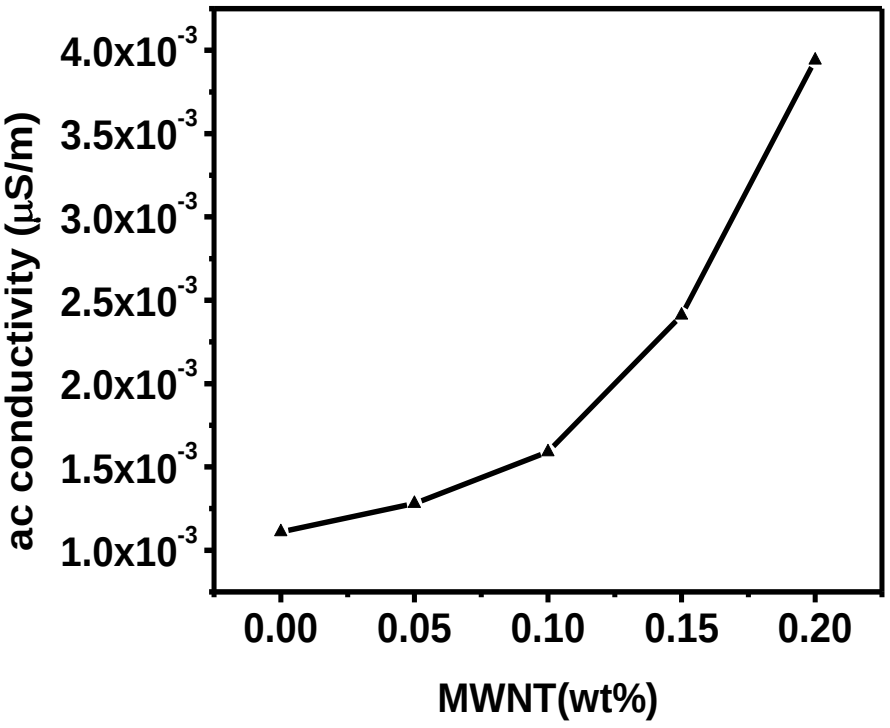

Figure 5.4: Variation of a.c. conductivity with different composites of PMMA/MWNT at 100 Hz

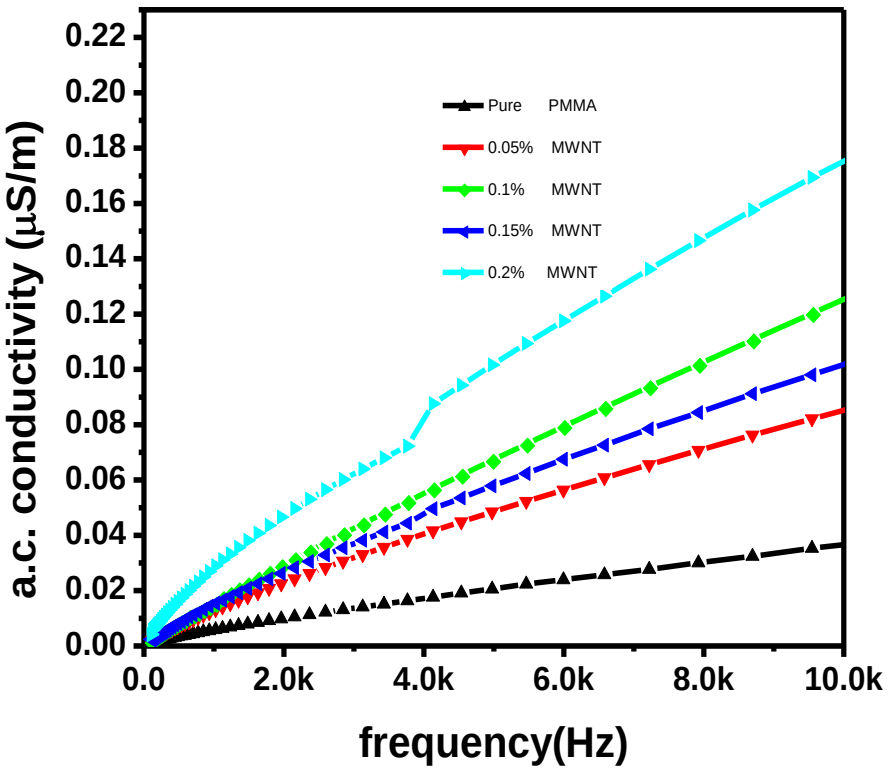

Figure 5.5: Variation of a.c. conductivity with frequency for different nanocomposites of PMMA/MWNT

It can be seen in Figure 5.5 that the conductivity of the PMMA and PMMA/MWNT nanocomposites increases with increasing frequency which is agreement with above equation (5.4). We also conclude from this Figure. that the conductivity σ_{ac} is increase with increasing MWNT concentration. It can be understood that by incorporation of multiwall carbon nanotube inside the polymer matrix, there is an increase in charge transport and the conductive grains of MWNT expend due to which mobility of carriers increase between the grains and hence a.c. conductivity increase. This type of behavior can be explained in terms of polarization effect and hopping. Improve charge transport property as well as electrical conduction and these MWNT/PMMA nanocomposites can be used as a good separating media [79,80].

5.4 Conclusion

This Chapter deals with dielectric properties of MWNT/PMMA nanocomposites. The dielectric properties of insulation polymer can be changed by dispersing small fillers such as carbon nanotube etc. Dielectric is important for explaining various phenomena in electronics, Optics and solid-state physics. The main aspect of research presented in this chapter investigates the dielectric properties of (Polymethyle methacrylate/Multiwall carbon nanotube) PMMA/MWNT nanocomposites and analyze the effect of MWNT loading.

To study the Dielectric properties of MWNT/PMMA nanocomposites, we measured the dielectric constant, a.c. conductivity, dielectric loss, and loss tangent. These all properties show the dielectric behavior of MWNT/PMMA nanocomposites. The dielectric behaviors of the nanocomposites were studied systematically over a range of frequencies to find the dependence of dielectric constant, dielectric loss tangent and dielectric strength on this parameter. Results show that electrical properties of these nanocomposites such as dielectric constant, dielectric loss, loss tangent and a.c. conductivity is changed with change in concentration of MWNT and with frequency of applied field and dielectric constant shows the dramatic enhancement in permittivity of these nanocomposites.

6.1 Conclusion

This Chapter describes conclusion and future scope for Positron Annihilation Spectroscopy for CNTs dispersed polymeric composite membranes and summarizes the various results which has been accomplished here. Based on the results and observations of the experiments that have been carried out, the following important conclusions are summarized.

The thesis is arranged into six Chapter, the first one giving an introduction to the thesis by describing the purpose of the study as well as the outline of the thesis.

In this first Chapter a brief review of the field is presented. Carbon nanotubes have extra ordinary properties like electrical, mechanical and thermal properties. These properties make nanotubes an excellent candidate for novel composite materials. Several previous studies focus on fabrication and characterization of carbon nanotube-polymer nanocomposites. Industrial applications of MWNT/PMMA composites have also been diversified to various fields including electronic devices and field emission display. Ultrasonication of solutions of polymers with dispersed nanotubes followed by solvent evaporation has been used successfully to achieve homogeneous nanocomposites.

Positron annihilation spectroscopy is a method that can be used to detect open volume defects and their chemical environments in a solid material. It is based on introducing positrons to a system where they eventually annihilate with electrons, their antiparticles. The annihilation of positron in condensed matter provides a unique way of obtaining information is transmitted through γ rays, emitted when the positron is annihilated in the material [43]. This chapter also introduces the concept and application of nanocomposites materials. Before the annihilation positrons can, due to their positive charge, get trapped at neutral and negative vacancies where the Columbic repulsion of the positive nucleus is missing. At the vacancy, the electron density is lower causing the increase in life time of positron in the sample, thus allowing positron lifetime measurement to characterize the open volume of defect. Since momentum is conserved in the annihilation, the annihilation photons contain

information about the electron momentum at the annihilation site. Doppler broadening spectroscopy (DBS) is the principal technique used to analyze the samples described in this research work. The technique examines the Doppler shift in the energy of the gamma radiation resulting from positron annihilation, which is linked to the momentum of the annihilating electrons, and thus properties of the material in which annihilation occur.

The areas of most concentrations are the center and the outer edges of the annihilation peak. Calculations are performed by comparing these areas to the total number of counts within the peak. The total momentum of the two photons is the same as the electron-positron system that produced the annihilation. When positrons enter a material, they thermalize quickly, within tens of picoseconds, through their interaction with the material. After they have lost a sufficient amount of energy, they are attracted to nearby electrons and annihilate. During the annihilation, the momentum of the positron is assumed negligible. Therefore, the amount of Doppler shift that occurs during each event is directly related to the energy of the electron [49]. The S-parameter is a ratio that compares the total number of points within the center region of the peak to the total number of counts within the peak. Another characteristic that could be measured using PAS is the Wing-parameter, or W-parameter, which compares the counts in the very outer regions of the peak to the total number of counts. Previous research work on positron annihilation has shown that the parameter can be used to help find defects in metals. The S-parameter is the ratio of peak counts to total counts in a curve of detected gamma radiation, representing low momentum positrons. The W-parameter is the ratio of the counts in the wings of the curve to the total, representing high momentum positrons.

Every material has a unique set of electrical characteristics that are dependent on its dielectric properties. As one of the most primarily used polymers in electronic industry is PMMA which has been of particular interest for embedded capacitor applications. The conductivity and dielectric properties of PMMA is changed by the addition of nanoparticles such as carbon nanotube etc. Dielectric materials play an

important role in defense data sensing navigation and communication through electric means. The dielectric parameters of such materials are therefore extremely important.

In the Chapter 2, the synthesis of carbon nanotube polymer nanocomposites used in various experimental technique are introduced. For the present work we have synthesized PMMA nanocomposites by following materials.

1. MWNT (Multi-walled carbon nanotube)
2. PMMA (Poly methyl methacrylate acid)

The MWNT/PMMA nanocomposites have been characterized by following techniques.

- Dialectical measurement
- XRD
- FT-IR
- I-V Characteristics
- Optical micrograph
- SEM measurement
- Doppler Broadening Spectroscopy

The fabrication of different concentration of PMMA nanocomposites by using above materials and their characterization technique, experimental and setups that were also described in this chapter.

In the Chapter 3, the Doppler broadening of annihilation radiation in PMMA/MWNT has been studied using ^{22}Na as a positron source. MWNT/PMMA nanocomposites membranes have been prepared by dispersing different concentrations (wt% - 0.05, 0.1, 0.15 and 0.2%) of multiwall carbon nanotubes (MWNT) in Poly methyl methacrylate (PMMA) matrix using benzene as a solvent. Fractional free volume is important in understanding gas transport through polymeric films. A polymer free volume is the difference between the specific polymer volume in the glassy or rubbery state and the volume associated with the crystalline solid at

the same temperature. Doppler broadening of annihilation radiation offer a sensitive method of defect characterization by measurement the momentum distribution technique. Doppler broadening spectrum technique is useful to define basic single value parameters which describe the shape of the peak.

The S- parameter and W- parameter were measured from the spectrum of different sample as a function of the relative weight. From this experiment we find out the behavior of the S- parameter and W- parameter in terms of positron annihilation and positronium formation for the various samples. Doppler broadening spectroscopy is direct correlate between these parameter and the various physical characteristics of Carbon nanotube.

Chapter 4 deals with characterization of MWNT/PMMA nanocomposites (wt% - 0.05, 0.1, 0.15 and 0.2) of multiwall carbon nanotubes (MWNT) in Poly methyl methacrylate (PMMA) matrix by electrical and optical properties studied at room temperature. Most of the nanoparticles are disperse into host matrixes to improve various properties. Among various nanoparticles, orientation of carbon nanotube in polymer matrix is one of the important task. Well dispersion carbon nanotube in polymer matrix can enhance the properties of the nanocomposites. X-ray diffraction is a useful tool to get structural information. In this chapter the samples are characterized by XRD, U-V visible, Optical micrograph, FT-IR, SEM measurement, Raman spectroscopy and I-V characteristics.

It is found that the conductivity measured in these MWNT/PMMA nanocomposites membranes is giving dramatically difference which is depends upon MWNT concentration in PMMA matrix. The dielectric constant was measured via MT-4080 Handheld precision LCR meter. Refractive index found to be increase and dielectric constant has been increased dramatically. The dispersion of the MWNT in PMMA was examined by optical microscopy and SEM measurement. UV-VIS spectra show that higher MWNTs concentration significantly decreases the transmittance of the MWNT-PMMA nanocomposites. Experimental results show here that CNT/polymer nanocomposite membranes can be used as a good charge separating media.

Chapter 5 deals with dielectric properties of MWNT/PMMA nanocomposites. The dielectric properties of insulation polymer can be changed by dispersing small fillers such as carbon nanotube etc. Dielectric is important for explaining various phenomena in electronics, Optics and solid-state physics. The main aspect of research presented in this chapter investigates the dielectric properties of PMMA/MWNT nanocomposites and analyze the effect of MWNT loading.

To study the Dielectric properties of MWNT/PMMA nanocomposites, we measured the dielectric constant, a. c. conductivity, dielectric loss, and loss tangent. These all properties show the dielectric behavior of MWNT/PMMA nanocomposites. The dielectric behaviors of the nanocomposites were studied systematically over a range of frequencies to find the dependence of dielectric constant, dielectric loss tangent and dielectric strength on these parameter. Results show that electrical properties of these nanocomposites such as dielectric constant, dielectric loss, loss tangent and a. c. conductivity is changed with change in concentration of MWNT and with frequency of applied field and dielectric constant shows the dramatic enhancement in permittivity of these nanocomposites.

Finally Chapter 6 deals with the summary of the work done during the tenure. It contains a brief description of the results obtained from various experiments. The results presented in the thesis demonstrate that Doppler broadening positron annihilation spectroscopy can discriminate among the MWNT/PMMA nanocomposites sample.

6.2 Future Work

Although a lot of work has already been done in the field of Positron Annihilation spectroscopy in polymer composites and CNT/polymer composites but much still remains to be looked into before it can really be put into practical use. The role of CNTs in polymer and their electric field alignment as per its contribution to the higher gas permeability through composite membrane. This not very clear at present and some more work is required to explore the use of CNTs as active material within the polymer host for many applications.

The test and analysis of CNT/polymer composites based membrane for many application is now in progress. We are also trying to analyze the effect of CNTs concentration, functionalization of CNTs with different organic acids in polymers by Positron Annihilationss. Hopefully we shall try in the near future.

References

[1] D. Chang, F. Huang and L. Cheng, *Polymer*. 44, 413 (2003).

[2] F. Kokai, K. Takahashi, M. Yudasaka, and S. Iijima, *J. Phys Chem. B* 104, 39 (2000).

[3] Al. Osaimil, N. Alhosiny, A. Badawi and S. Abdallah, *International Journal of Engineering & Technology*. 13, 2 (2013).

[4] S. Iijima *Nature* 354, 56 (1991).

[5] J. Wang, V. O. Jobando and C. A. Quarles, *Mater. Sci. Forum.* 607, 186 (2009).

[6] G. Yang, R. Teng and P. Xiao, *Polym. Compos.* 18, 477 (1997).

[7] D. Lin, C. Chang, F. Huang and L. Cheng, *Polymer*. 44, 413 (2003).

[8] M. Baibarac and P. Gómez-Romero, *J. nanoscience and nanotechnology*. 6, 14 (2006).

[9] G. Bottino, E. Capannelli and A. Comite, *Desalination.* 35, 146 (2002).

[10] H. Tawansi, Y. Zidan, M. Moustafa and A. H. Eldumiaty, *Phys. Script.* 55, 243 (1997).

[11] T. D. Fornes, J. W. Baur, Y. Sabba and E. L. Thomas, *Polyme.* 47, 1704-1714 (2006).

[12] V. I. Grafutin, E. P. Prokop, *Brazilian journal of Science.* 35, 3 (2005).

[13] C. Palacio, A. Djourelov, J. Kuriplach, C. Dauwe, N. Laforests and D. segers, *phys. Stat.sol. (c)* 4, 10 (2007).

[14] J. K. W. Sandler, *Polymer*. 45, 2001- 2015 (2004).

[15] S. Srivastava, S.S. Sharma, Shweta Agrawal, Sumit Kumar, M. Singh and Y.K. Vijay, *Synthetic Metals.* 160, 529-534 (2010).

[16] M. Debowska, J. Rudzinska and A. Pasternath 1996 *Acta Phys Polonica A.* 95 509 (1996).

[17] V. T. Truong, K. M. C. Tsang, S. J. Keough, St John, N.A. Proceedings of SPIE The International society for optical engineers. 6415, 641503-641503-9 (2006).

[18] M. Bratcher, B. Gersten, H. Ji, J. Mays Materials Research Society symposia proceedings. 706, 323-328 (2002).

[19] R. Lopez-castanares, O. Olea-Cardoso and F. Vazquez-Moreno, *Bulg. J. Phys.* 29, 155 (2002).

[20] J. Xu and J. Moxon, *J. Radiat. Phys. Chem.* 68, 239 (2003).

[21] F. Faupel, J. Kanzow, P. Sperr and G. Gel, *J. Mater. Sci. Forum.* 219, 445 (2004).

[22] J. Borek and W. Osoba, *J. Polym. Sci. Part B: Polym. Phys.* 36, 1839 (1998)

[23] Safadi, R. Andrews and E. A. Grulke, *Journal of applied polymer science*. 84, 2660-2669 (2002).

[24] J. P. Salvetat, A. D. Briggs, J. M. Bonard, R. R. Bacsa and A. J. Kulik, *Physical Review Letters.* 82, 944-947 (1999).

[25] O. Probst, E. Moore, D. Resasco, B. Grady, *Polym.* 45, 4437- 4443 (2004).

[26] G. Zhan, J. A. Nichols, D. A. Dixon, *J. Phys. Chem.* A 107, 4184 (2003).

[27] Morin, D. Simon, R. Sautet, *J. Phys. Chem.* B 107, 2995 (2003).

[28] H. F. M. Mohamed, E. E. Abdel-Hady, H. B. Alaa, *Mater Sci Forum.* 328, 445 (2004).

[29] M.E. Semaana, C.A. Quarlesb, Leszek Nikiel, *Polymer Degradation and Stability.* 75, 259–266 (2002).

[30] H.F.M. Mohamed, Gomaa G. Abd-Elsadek *radiation physics and chemistry.* 58, 597-601 (2000).

[31] T. Jeevanda, O. G. Palanna. Joong Hee Lee, Siddaramaiah and Ranganathaiah, *Advance Material Research.* 123 59-62 (2010).

[32] V. Nascimento, and R. Helene, *Nanomaterials, Applications and Properies.* 2, 125 (2011).

[33] Sharma, B. Tripathi, and Y. K. Vijay, *J. Membr. Sci.* 361, 89 (2010).

[34] S. Srivastava, S. S. Sharma, S. Kumar, M. Singh, and Y. K.Vijay, *International journal of hydrogen Energy.* 3, 8444-8450 (2009).

[35] M. Bratcher, B. Gersten, and H. Ji, *J. Materials Research Society symposia proceedings.* 706, 323-328 (2002).

[36] D.C. Tiwari, S. Vikas and R. Sharma, *Indian journal of pure & Applied phy*. 50, 49-56 (2012).

[37] T. Estabrak, N. Naje, *Indian journal of science and Technology.* 47, 731-735 (2011).

[38] H. F. M. Mohamed, E. E. Abdel-Hady and H. B. Alaa, *Mater. Sci. Forum.* 328, 445 (2004).

[39] W. C. Hao, F. Pan, T. M. Wang, C. L. Zhou and L. Wei, *Chin. Phys. Lett.* 23, 223 (2006).

[40] A. Dupasquier, G. Kögel and A. Somoza, *Acta Materialia.* 52, 4707-4726 (2004).

[41] M. Eldrup, K. O. Jensen, *Phys. Stat. Sol. (a)* 102, 145 (1987).

[42] A. P. Srivastava, and S.K. Shrivastava, *Indian J. Pure & Appl. Phy* 19**,** 953 (1981).

[43] A. K. Saraswat and D. C. Dube, *Indian J. Pure & Appl. Phy*. 36 737 (1990)

[44] P. Scherrer, Gottinger Nachrichten, 2, 98 (1998).

[45] R. M. Nieminen and J. Oliva, *Phys. Rev. B* 22, 2226 (1980).

[46] S. Valkealahti and R. M. Nieminen, *Appl. Phys. A* 35, 51 (1984).

[47] K. Vehanen, P. Saarinen, P. Hautojärvi and H. Huomo, *Phys. Rev. B* 35, 4606 (1987).

[48] P. Krause, G. Pötschke and L. Häubler, *Compos. Sci. Technol.* 69, 1505 (2009).

[49] M. Misheva, N. Djourelov and J. Z. V. Kotharova, *Thin Solid Films*. 283, 26 (1996).

[50] F. J. Balta-Calleja, J. M. Salazar and H. Cackovic *J. mater Sci.* 16 739 (1981).

[51] D. Lin, C. Chang, F. Huang and L. Chenge *Polymer*. 44, 413 (2003).

[52] L. Yan and S. Xiander *J. Membr Sci.* 276 162 (2006)

[53] A. Patnaik, Z. Zhu, G. Yong and Y. Sun, *Phys Stat Solidi(a*) 169, 115 (1998).

[54] M. Debowska, J. Rudzinska and A. Pasternath *Acta Phys Polonica.* 95 509 (1996).

[55] B. D. Kuriakose, S. K. Bhagawan, S. S. Sivaramkrishnan and R. Athithan, *J. Appl. Polym. Sci.* 32, 5509 (1986).

[56] M. Moniruzzaman and K. I. Winey, 39, 5194 (2006).

[57] K. Mylavganam and L. C. Zhang, *Recent Patents Nanotechnol.* 56, 59 (2007).

[58] M. Ge and K. Sattler, *J. Appl. Phys. Lett.* 64, 710 (1994).

[59] S. Allaoui and H. M. Cheng, *J. Compos. Sci. Technol.* 62, 1993 (2002).

[60] H. Geng, R. Rasen, B. Zheng and H. Shimoda, *Adv. Mater.* 14, 1387 (2002).

[61] S. Cui, R. Canet, A. Derre, M. Couzi and P. Delhaes, *Carbon.* 41, 797 (2003).

[62] M. Cadek, J. N. Coleman, and V. Barron, *Appl. Phys. Lett.* 81, 5123 (2002).

[63] T. Tauc and S. Memth . *J. Non-Cryst Solids.* 126, 596 (1972).

[64] B. A. Hasan, *Journal of Education College*. 56, 4644, (2005).

[65] M. A. Lo'pez, Manchado and L. Valentini, *Carbon.* 43, 1499 (2005).

[66] Dresselhauss and P. Avouris, Springer, Berline, Germany (2001).

[67] E. Camponeschi, R. Vance, M. Al-Haik, H. Garmestani and R. Tannenbaum, *Carbon.* 45, 2037 (2007).

[68] S. Kirkpatrick, *Rev. Mod. Phys.* 45, 574 (1973).

[69] M. Yu, H. H. Fumke, J. L. Falconer, and R. D. Noble, *Nano Lett.* 9, 225 (2008).

[70] Verweij and M. C. Schillo, and J. Li, *Small.* 3, 1996 (2007).

[71] C. Dekker, *Physics Today.* 52, 22 (1999).

[72] M. Endo, T. Hayashi, Y. A. Kim, M. Terrones, and M. S. Dresselhaus, *Philos. Trans. R. Soc. London, Ser. A* 362, 2223 (2004).

[73] R. H. Baughman, A. A. Zakhidov and W. A. de Heer, *Science.* 297, 787 (2002).

[74] W. S. Kim, H. S. Song, B. O. Lee, K. H. Kwon, Y. S. Lim, and M. S. Kim, *Macromol. Res.* 10, 253 (2002).

[75] J. K. W. Sandler, J. E. Kirk, I. A. Kinloch, M. S. P. Shaffer, and A. H. Windle, *Polymer*. 44, 5893 (2003).

[76] V. Bobnar, A. Levstik, C. Huang, and Q. M. Zhang, *J. Non- Crystalline Solids.* 353, 205 (2007).

[77] S. L. Shi, L. Z. Zhang and J. S. Li, *J. Polym. Res.* 16, 395 (2009).

[78] V. I. Grafutin, E. P. Prokopev, Uspekhi Fizicheskikh Nauk, *Russian Academy of Sciences.* Physics-Uspekhi 45, 59-74 (2002).

[79] M. Eldrup, Defects in Solids, edited by Chadwick, A. V., Terenzi, M., Plenum Publishing Corporation, (1986).

[80] Mars E. Semaana, C.A. Quarlesb, Leszek Nikiel, *Polymer Degradation and Stability.* 75, 259–266 (2002).